The quantum needle of the avian magnetic compass

Hamish G. Hiscock[a,1], Susannah Worster[a,1], Daniel R. Kattnig[a], Charlotte Steers[a], Ye Jin[a], David E. Manolopoulos[a], Henrik Mouritsen[b,c] and P. J. Hore[a,2]

[a]Department of Chemistry, University of Oxford, Physical & Theoretical Chemistry Laboratory, Oxford OX1 3QZ, UK
[b]Institut für Biologie und Umweltwissenschaften, Carl von Ossietzky Universität Oldenburg, 26111 Oldenburg, Germany
[c]Research Centre for Neurosensory Sciences, University of Oldenburg, 26111 Oldenburg, Germany

[1]These authors contributed equally to this work.
[2]To whom correspondence may be addressed. E-mail: peter.hore@chem.ox.ac.uk

Keywords

magnetic compass | magnetoreception | migratory birds | quantum biology | radical pair mechanism

Author contributions

P.J.H. designed the research; H.G.H, S.W. and D.R.K. performed the research; C.S. and J.Y. performed preliminary calculations; H.G.H, S.W., D.R.K., D.E.M., H.M. and P.J.H. discussed the results and their interpretation; P.J.H., H.M. and D.E.M. wrote the manuscript. All authors read and commented on the manuscript.

Abstract

Migratory birds have a light-dependent magnetic compass, the mechanism of which is thought to involve radical pairs formed photochemically in cryptochrome proteins in the retina. Theoretical descriptions of this compass have so far been unable to account for the high precision with which birds are able to detect the direction of the Earth's magnetic field. Here we use coherent spin dynamics simulations to explore the behaviour of realistic models of cryptochrome-based radical pairs. We show that when the spin-coherence persists for longer than a few microseconds, the output of the sensor contains a sharp feature, referred to as a 'spike'. The spike arises from avoided crossings of the quantum mechanical spin energy-levels of radicals formed in cryptochromes. Such a feature could deliver a heading precision sufficient to explain the navigational behaviour of migratory birds in the wild. Our results: (a) afford new insights into radical pair magnetoreception, (b) suggest ways in which the performance of the compass could have been optimised by evolution, (c) may provide the beginnings of an explanation for the magnetic disorientation of migratory birds exposed to anthropogenic electromagnetic noise, and (d) suggest that radical pair magnetoreception may be more of a 'quantum biology' phenomenon than previously realised.

Significance

Billions of birds fly thousands of kilometres every year between their breeding and wintering grounds helped by an extraordinary ability to detect the direction of the Earth's magnetic field. The biophysical sensory mechanism at the heart of this compass is thought to rely on magnetically sensitive, light-dependent chemical reactions in cryptochrome proteins in the eye. So far, no theoretical model has been able to account for the $< 5^\circ$ precision with which migratory birds are able to detect the geomagnetic field vector. Here, using computer simulations, we show that genuinely quantum mechanical, long-lived spin coherences in realistic models of cryptochrome can provide the necessary precision. The crucial structural and dynamical molecular properties are identified.

Introduction

Migratory birds have a light-dependent magnetic compass (1-4). The primary sensory receptors are located in the eyes (2, 3, 5-7) and directional information is processed bilaterally in a small part of the forebrain accessed via the thalamofugal visual pathway. The evidence currently points to a chemical sensing mechanism based on photo-induced radical pairs in cryptochrome flavoproteins in the retina (8-18). Anisotropic magnetic interactions within the radicals are thought to give rise to intracellular levels of a cryptochrome signalling state that depend on the orientation of the bird's head in the Earth's magnetic field (8, 9, 19). In support of this proposal, the photochemistry of isolated cryptochromes *in vitro* has been found to respond to applied magnetic fields in a manner that is quantitatively consistent with the radical pair mechanism (15). Aspects of the radical pair hypothesis have also been explored in a number of theoretical studies, the majority of which have concentrated on the *magnitude* of the anisotropic magnetic field effect (9, 10, 16, 17, 19-27). Very little attention has been devoted to the matter we address here — the *precision* of the compass bearing available from a radical pair sensor (28).

To migrate successfully over large distances, it is not sufficient simply to distinguish north from south (or poleward from equatorward (29)). A bar-tailed godwit (*Limosa lapponica baueri*), for example, was tracked by satellite flying from Alaska to New Zealand in a single 11,000 km non-stop flight across the Pacific Ocean (30). A directional error of more than a few degrees could have been fatal. Since the magnetic compass seems to be the dominant source of directional information (31), and

the only compass available at night under an overcast (but not completely dark) sky, migratory birds must be able to determine their flight direction with high precision using their magnetic compass. Studies have shown that migratory songbirds can detect the axis of the magnetic field lines with an accuracy better than 5° (32, 33). Any plausible magnetoreception hypothesis must be able to explain how such a directional precision can be achieved. Previous simulations of radical pair reactions (e.g. (9, 10, 17, 20, 21)) show only a weak dependence on the direction of the geomagnetic field and therefore cannot straightforwardly account for the magnetic orientation of birds in the wild.

Theoretical treatments of radical-pair-based magnetoreception typically involve simulations of the quantum spin dynamics of short-lived radicals in Earth-strength (ca. 50 μT) magnetic fields (9, 10, 17). The general aim is to determine how the yield of a reaction product depends on the orientation of the reactants with respect to the magnetic field axis. A crucial element in all such calculations is the presence of nuclear spins whose hyperfine interactions are the source of the magnetic anisotropy (8, 16). Most studies have focussed on idealised spin systems comprising the two electron spins, one on each radical, augmented by one or two nuclear spins (9, 21-27, 34). Only a handful has attempted to deal with realistic, multinuclear radical pairs (10, 16, 17, 20). The other critical ingredient in such simulations is the lifetime of the electron spin-coherence: if the spins dephase completely before the radicals have a chance to react, there can be no effect of an external magnetic field (35). Several studies have assumed, explicitly or implicitly, that the spin-coherence persists for about a microsecond, i.e. the reciprocal of the electron Larmor frequency (1.4 MHz) in a 50 μT field (9, 10, 17, 20). Either because the spin system was grossly oversimplified (9, 21-27, 34), or because of this restriction on the spin-coherence time, previous theoretical treatments have generally predicted the reaction yield to be a gently varying (often approximately sinusoidal) function of the orientation of the radical pair in the geomagnetic field. Although capable of delivering information on the direction of the field, such a compass would not provide a precise heading. A more sharply peaked dependence on the field direction would be needed to achieve a compass bearing with an error of 5° or less.

Here, we explore the behaviour of cryptochrome-inspired radical pairs with multinuclear spin systems and long-lived (> 1 μs) spin-coherence. We conclude that there is ample scope for a cryptochrome-based radical pair compass to have evolved with a heading precision sufficient to explain the navigational behaviour of migratory birds both in the laboratory and in the wild.

Results

Spin dynamics simulations. Product yields of radical pair reactions were calculated as described elsewhere (10, 16, 36-38) by solving a Liouville equation containing (a) the internal magnetic (hyperfine) interactions of the electron spin with the nuclear spins in each radical, (b) the magnetic (Zeeman) interactions of the two electron spins with the external magnetic field, and (c) appropriate spin-selective reactions of the singlet and triplet states of the radical pair.

As a starting point, we modelled [$FAD^{\bullet-}$ $TrpH^{\bullet+}$], the radical pair that is responsible for the magnetic sensitivity of isolated cryptochrome molecules *in vitro* (15). It consists of the radical anion of the non-covalently bound flavin adenine dinucleotide (FAD) cofactor and the radical cation of the terminal residue of the 'tryptophan (Trp) triad' electron transfer chain within the protein (39-41). All calculations were performed in a coordinate system aligned with the tricyclic flavin ring system (Fig. 1A): *x* and *y* are respectively the short and long in-plane axes and *z* is normal to the plane. Hyperfine interaction tensors were calculated by density functional theory (Supporting Information (SI Appendix, Section S1). Following Lee *et al*. (16), the 14 largest hyperfine interactions, 7 in $FAD^{\bullet-}$ and 7 in $TrpH^{\bullet+}$, were included. (See SI Appendix, Section S2 for additional simulations including up to 22

nuclear spins.) A magnetic field strength of 50 μT was used throughout. The relative orientation of the two radicals was that of FAD and Trp-342 in *Drosophila melanogaster* cryptochrome (PDB entry 4GU5) (SI Appendix, Section S1) (42, 43). The initial state of the spin system was a pure singlet. Two approximations (SI Appendix, Sections S3 and S4) were introduced to make simulations of the 16-spin system computationally tractable (9): (a) exchange and dipolar interactions between the radicals were assumed to be negligible, and (b) the singlet and triplet states were assumed to react to form distinct products with identical first order rate constants, *k*. The lifetime of the radical pair, τ, is defined as the reciprocal of *k.* As a measure of the available directional information, we calculated Φ_S, the fractional yield of the product formed from the singlet state of the radical pair after the reactions have proceeded to completion (10, 16). Spin relaxation processes were not included in the initial simulations. Further details are given in the SI Appendix, Section S5.

Flavin-tryptophan radical pair. Fig. 1B shows the variation of Φ_S for [$FAD^{\bullet-}$ $TrpH^{\bullet+}$] as the direction of a 50 μT magnetic field, specified by the angle θ, is rotated in the *zx*-plane of the flavin. When θ = 0, the field is parallel to the flavin *z*-axis (Fig. 1A). With a lifetime τ = 1 μs, Φ_S exhibits a shallow minimum around θ = 90° and maxima near 0° and 180°, as found previously (16). Shorter lifetimes gave even weaker angular variation. As the lifetime is prolonged from 1 μs towards 100 μs, the dependence of Φ_S on θ becomes increasingly structured and a prominent 'spike' emerges, strengthens and narrows. Centred accurately at θ = 90°, this feature occurs when the magnetic field is in the plane of the flavin ring system (parallel to the *x*-axis). As τ is increased beyond 100 μs, the only change is that the spike grows (by roughly a factor of three as $\tau \to \infty$).

The anisotropy of Φ_S can be seen more clearly from polar plots of the same data (Fig. 1C) after subtraction of the isotropic components. As the lifetime is prolonged, the anisotropy grows and Φ_S depends more strongly on θ. As expected from time-reversal symmetry, Φ_S is invariant to inversion of the direction of the magnetic field, a property shared by the avian magnetic compass (29). Very similar behaviour was found when the magnetic field was rotated in the molecular *zy*-plane. In fact, Φ_S has roughly axial symmetry around the molecular *z*-axis, apart from a tilted feature arising predominantly from the indole nitrogen of $TrpH^{\bullet+}$, as may be seen from the three-dimensional polar plot in Fig. 1D (τ = 10 μs). The spikes in Figs 1B and 1C at θ = 90° are, in fact, cross sections through the thin equatorial disk found produced when the magnetic field axis is close to the *xy*-plane of the flavin (Fig. 1D).

Fig. 1E shows ' visual modulation patterns' (9, 19, 28) calculated for the same radical pair as Figs 1B–D (details in the SI Appendix, Section S6). They are representations of a bird's perception of the directional information delivered by an array of cryptochrome-containing magnetoreceptor cells distributed around the retina, in this case for a bird in the northern hemisphere looking horizontally towards magnetic north in a 50 μT magnetic field with a 66° inclination. As the lifetime τ is prolonged, and the spike becomes stronger, so the 'spot' that indicates the axis of the geomagnetic field lines becomes more intense and less diffuse. It is not hard to imagine that the patterns in Fig. 1E for $\tau \geq 5$ μs would give more precise compass headings than that for τ = 1 μs.

Finally, a degree of rotational disorder amongst the magnetoreceptor cells (19, 28) can be modelled by averaging the polar plot in Φ_S (Fig. 1D) over a 360° rotation around a chosen axis (SI Appendix, Section S6). If this axis is in the *xy*-plane of the flavin, the thin blue equatorial disk in Fig. 1D turns into the needle-shaped object (Fig. 1E, τ = 10 μs) that appears to be ideal for determining a precise compass bearing. As mentioned above, a radical pair sensor is an *inclination*, rather than a *polarity*,

compass so that the resemblance of Fig. 1E to a magnetized compass needle should not be taken too literally.

Origin of the spike in Φ_S. The approximate axial symmetry of Φ_S for τ = 1 μs (Fig. 1C) has been noted before and was attributed principally to the two nitrogens, N5 and N10, in the central ring of the $FAD^{\bullet-}$ radical (10, 16). These are the only nuclei in [$FAD^{\bullet-}$ $TrpH^{\bullet+}$] with hyperfine tensors that, like Φ_S, are approximately axially symmetric around the flavin *z*-axis. It therefore seems probable that they also play a role in creating the spike that arises when τ > 5 μs.

This is confirmed by Fig. 2A which shows Φ_S for a very slightly modified version of [$FAD^{\bullet-}$ $TrpH^{\bullet+}$]. The *z*-components of the hyperfine interactions of N5 and N10 in flavin radicals are large and the *x* and *y*-components have small but non-zero absolute values (SI Appendix, Section S7). The calculated principal values of the two interactions are: (A_{xx}, A_{yy}, A_{zz}) = (−0.087, −0.100, 1.757) mT for N5 and (−0.014, −0.024, 0.605) mT for N10 (SI Appendix, Section S1; here 1 mT corresponds to 28 MHz). When A_{xx} and A_{yy} for either N5 or N10 were set to zero, the spike was attenuated by 60-70%; when A_{xx} and A_{yy} for *both* nitrogens were set to zero, the spike disappeared (Fig. 2A). The rest of Φ_S remained essentially unchanged. The strong, sharp component of Φ_S for [$FAD^{\bullet-}$ $TrpH^{\bullet+}$] therefore owes its existence, at least in part, to the form of the hyperfine tensors of N5 and N10 in the flavin radical, i.e. large A_{zz} and small but non-zero $|A_{xx}|$ and $|A_{yy}|$.

The SI Appendix, Section S8 contains an analysis that unambiguously attributes the thin equatorial disk in Fig. 1D to avoided crossings of the quantum mechanical energy levels of the radical pair spin Hamiltonian as a function of the magnetic field direction and predicts that the lineshape of a cross section through the disk (i.e. the spike) will be an inverted Lorentzian. When A_{xx} and A_{yy} for both nitrogens are set to zero, the avoided crossings become level crossings and the spike vanishes.

Simpler flavin-containing radical pairs. To obtain further insight into the origin of the spike, simulations were performed for three radical pairs related to [$FAD^{\bullet-}$ $TrpH^{\bullet+}$]. (1) When the $TrpH^{\bullet+}$ radical was replaced by a hypothetical radical which had no hyperfine interactions, Φ_S was found to vary smoothly and approximately sinusoidally with θ and barely changed as τ was increased from 1 μs to 100 μs (SI Appendix, Section S9). (2) This pattern (gentle, smooth θ-dependence, no spike) persisted when a single *isotropic* hyperfine interaction was present in the second radical (SI Appendix, Section S9). (3) However, when the second radical contained an axially *anisotropic* hyperfine interaction with $A_{xx} = A_{yy} = 0$ or $A_{xx} = A_{yy} \neq 0$, the spike at θ = 90° reappeared and, as in Fig. 1B, strengthened with increasing lifetime (Fig. 2B). From this and other simulations of flavin-containing radical pairs it appears that an additional condition for the existence of the spike is that the radical that partners the $FAD^{\bullet-}$ should have at least one nucleus with an anisotropic hyperfine interaction. This condition is amply fulfilled by $TrpH^{\bullet+}$ in which the indole nitrogen and the aromatic hydrogens all interact anisotropically with the electron spin (16).

A toy radical pair. To confirm and further explore these conclusions, we devised a 'toy' radical pair, with a smaller, more manageable spin system, that behaves qualitatively like [$FAD^{\bullet-}$ $TrpH^{\bullet+}$]. One radical ($X^{\bullet}$) had a single nitrogen with a hyperfine tensor similar to that of the N5 in $FAD^{\bullet-}$. The other ($Y^{\bullet}$) had a single nitrogen with an axial hyperfine tensor modelled on the indole nitrogen in $TrpH^{\bullet+}$. Like [$FAD^{\bullet-}$ $TrpH^{\bullet+}$], [$X^{\bullet}$ $Y^{\bullet}$] shows a spike at θ = 90° superimposed on a rolling background (Fig. 2C). The spike became more pronounced when either the lifetime was prolonged or the amplitudes of the small transverse hyperfine components in $X^{\bullet}$ were increased. For example, doubling A_{xx} and A_{yy}

when τ = 10 μs increased the amplitude of the spike by about the same amount as increasing τ from 10 μs to 33 μs without changing A_{xx} and A_{yy} (Fig. 2C).

Spin relaxation in the toy radical pair. Of course, the spin-coherence does not persist indefinitely but inevitably relaxes towards the equilibrium state in which all spin-correlation has vanished. The rate of this process is highly relevant because there can be no magnetic field effect if the spin system equilibrates before the radicals react. The dominant spin relaxation pathways in a cryptochrome-based radical pair probably arise from modulation of hyperfine interactions by low-amplitude stochastic librational motions of the radicals within their binding pockets in the protein. The approach to equilibrium is likely to be highly complex for realistic radicals undergoing realistic motions especially because the external magnetic field is weaker than many of the hyperfine interactions. In general, one can expect a multitude of relaxation pathways, at a variety of rates, not all of which necessarily degrade the performance of the radical pair as a compass sensor (44).

To explore the conditions necessary for the spike to survive in the presence of molecular motion, we studied a simple model of the microscopic dynamics of the $FAD^{\bullet-}$ radical in cryptochrome. The tricyclic isoalloxazine moiety was allowed to undergo rotational jumps ($+\beta \leftrightarrow -\beta$ degrees) around its *y*-axis with a first order rate constant, k_r (SI Appendix, Section S10). In the language of magnetic resonance, this rocking motion constitutes a 'symmetric two-site exchange' process (45), the effect of which is to modulate the hyperfine field experienced by the electron spin. For a given set of anisotropic hyperfine interactions, the only additional parameters are the rocking angle and the rate constant.

To get an initial idea of the expected behaviour, we started with the toy radical pair introduced above. Fig. 3A shows Φ_S when $Y^{\bullet}$ is stationary and $X^{\bullet}$ undergoes 10° rotational jumps (i.e. β = 5°) around its *y*-axis. The lifetime of the radical pair was fixed at 10 μs, so that any relaxation pathway occurring on this timescale, or faster, could influence Φ_S. When the rocking is sufficiently fast ($k_r \geq 3 \times 10^9$ s^{-1}, Fig. 3A), the differences in the magnetic interactions in the two orientations are averaged by the motion and a single sharp spike is seen at θ = 90°. As k_r is reduced, the averaging becomes less efficient, causing attenuation of the spike (without significant broadening) and flattening of the gently varying background (Fig. 3A and SI Appendix, Section S11). Spin-relaxation is most efficient when k_r is comparable to the strengths of the hyperfine interactions, i.e. $\approx 10^8$ s^{-1}. Under these conditions, Φ_S tends towards 0.25, the statistical singlet fraction expected at thermal equilibrium.

These simulations were performed for a rocking axis (*y*) perpendicular to the symmetry axis (*z*) of the hyperfine tensor in $X^{\bullet}$. Rotation around an axis tilted out of the *xy* plane results in less extensive modulation of the magnetic interactions, less efficient spin relaxation, and less attenuation of the spike for a given k_r. In this respect, Fig. 3A represents the worst case. The behaviour of Φ_S when $k_r \leq 10^8$ s^{-1} is discussed in the SI Appendix, Section S12.

In summary, the spike survives if $k_r \geq 3 \times 10^9$ s^{-1} (Fig. 3A). This value corresponds to a librational wavenumber of the aromatic ring systems greater than ca. 0.1 cm^{-1}.

Spin relaxation in a flavin-containing radical pair. We now look at the effects of motion on a more realistic spin system. It proved impractical to repeat the above calculation for the full (16-spin) [$FAD^{\bullet-}$ $TrpH^{\bullet+}$] radical pair treated above. Instead, we studied [$FAD^{\bullet-}$ $Y^{\bullet}$] in which $FAD^{\bullet-}$ contained 7 nuclear spins (as above) and $Y^{\bullet}$ was the same as in the toy radical pair, [$X^{\bullet}$ $Y^{\bullet}$]. Fig. 3B shows Φ_S for [$FAD^{\bullet-}$ $Y^{\bullet}$] with the $FAD^{\bullet-}$ radical undergoing 10° rotational jumps (β = 5°) around its *y*-axis with rate

constants in the fast exchange regime: $10^9\ s^{-1} \le k_r \le 3 \times 10^{11}\ s^{-1}$. As was the case for [$X^\bullet$ $Y^\bullet$] (Fig. 3A), when τ = 10 μs the spike at θ = 90° persisted for rocking rates down to $3 \times 10^9\ s^{-1}$ and is even visible when $k_r = 10^9\ s^{-1}$. Similar behaviour was found for a [$X^\bullet$ $TrpH^{\bullet+}$] pair in which $TrpH^{\bullet+}$ underwent 10° jumps (SI Appendix, Section S13). Spin relaxation effects were more pronounced for jumps larger than 10°.

Clearly, the dynamics of $FAD^{\bullet-}$ and $TrpH^{\bullet+}$ in cryptochrome are considerably more complicated than this two-site jump model. However, we can infer from these exploratory studies that the spike in Φ_S is not excessively sensitive to reasonably rapid, relatively low-amplitude motions of the type likely to occur for the radicals in their binding sites in cryptochrome. The message we take from these calculations is that radical motions on timescales faster than about 1 ns could allow the spikiness of Φ_S to survive.

Precision of the compass bearing. The directional information available from Φ_S will inevitably be degraded by stochastic noise in the detection system (46). We can anticipate that for a given noise level, a sharper and stronger spike will deliver a more precise compass bearing. In the SI Appendix, Section S14, we attempt to quantify the effects of detector noise on the signals in Fig. 1. It is shown that to obtain a precision of 1° when τ = 1 μs the noise level would have to be ca. 40 times smaller than when τ = 10 μs. If such an improvement in signal-to-noise had to be achieved by averaging repeated measurements, it would take ca. 40^2 = 1600 times longer for a radical pair with a lifetime of 1 μs than for one with 10 μs. Put another way, a bird might be able to obtain a ±1° compass bearing in, say, 1 s instead of 30 min or by employing ca. 1600 times fewer cryptochrome molecules, if τ were 10 μs rather than 1 μs.

Discussion

We have demonstrated that a radical pair magnetoreceptor may be capable of much higher angular precision than previously thought possible. More specifically, we have presented a version of the radical-pair model that could potentially explain the magnetic compass precision observed for night-migratory songbirds (32, 33). The feature that makes this feasible, referred to as a spike, emerges naturally for cryptochrome-based radical pairs when the lifetime of the spin-coherence exceeds 1 μs.

FAD radical. A fundamental requirement for the occurrence of a pronounced spike in the reaction yield (Φ_S) is that one of the radicals is $FAD^{\bullet-}$ or at least something closely resembling it. In particular, the two nitrogen nuclei (N5 and N10) in the central ring of the tricyclic flavin ring system appear to have almost ideal magnetic hyperfine interactions (16). The width and height of the spike can be tuned by adjusting the transverse components (A_{xx} and A_{yy}) of these interactions (some experimental values are given in the SI Appendix, Section S7), implying that random mutations in the sequence of the protein in the neighbourhood of the FAD could have provided evolution with the scope to optimise the compass precision. We emphasize that the precise values of the hyperfine parameters required to produce a substantial spike in Φ_S are not crucial and were neither guessed nor carefully chosen; they came directly from independent molecular orbital calculations (performed several years before we embarked on the present work (47)).

Partner radical. A second prerequisite for spiky behaviour is that the radical that partners the $FAD^{\bullet-}$ must have at least one appreciably anisotropic hyperfine interaction. This condition is certainly satisfied by the $TrpH^{\bullet+}$ radical formed by photo-induced electron transfer along the Trp-triad in cryptochrome, as our simulations have demonstrated. It is also consistent with the oxidised form of

ascorbic acid ($Asc^{\bullet-}$), a radical that has been tentatively suggested (but for which there is currently no evidence) as an alternative to $TrpH^{\bullet+}$, on the basis that [$FAD^{\bullet-}$ $Asc^{\bullet-}$] is expected to show much larger magnetic field effects than [$FAD^{\bullet-}$ $TrpH^{\bullet+}$] by virtue of the small hyperfine interactions in $Asc^{\bullet-}$ (16). (See Ref. (16) for a more detailed discussion of possible partner radicals.) However, a spike would not be expected for a [$FAD^{\bullet-}$ $Z^{\bullet}$] radical pair, in which $Z^{\bullet}$ is a radical completely devoid of hyperfine interactions, such as superoxide, $O_2^{\bullet-}$ (even if its spin relaxation could be made slow enough (48, 49)). Such a radical pair was originally proposed to explain the reported inability of European robins (*Erithacus rubecula*) to use their magnetic compass when exposed to a narrow-band radiofrequency field at the Larmor frequency (1.4 MHz for a 50 μT geomagnetic field) (50). However, very recent experiments (51), designed to replicate the earlier study (50) under much more stringently controlled conditions, failed to find specific effects at the Larmor frequency. In contrast, very weak broadband fields were found to disrupt the birds' magnetic compass orientation capabilities (51, 52). These new findings are consistent with radical pairs that have significant hyperfine interactions in both radicals, e.g. [$FAD^{\bullet-}$ $TrpH^{\bullet+}$] and [$FAD^{\bullet-}$ $Asc^{\bullet-}$].

Spin relaxation and magnetic disorientation. The third major condition for the emergence of the spike is that the spin-coherence times of the radicals should be longer than 1 μs, which in turn means that the librations of the radicals within their binding pockets must be of relatively low amplitude and not too sluggish. As such motions are determined by the interactions of the radicals with the protein environment, this is another property that could have been optimised by evolution. Spin relaxation much slower that 1 μs has been invoked before to explain the apparent sensitivity of birds to weak (nanotesla) monochromatic radiofrequency fields (21, 26, 53, 54). The problem with this proposal is that if there is no possibility of a spike, a coherence time of 1-2 μs is sufficient to achieve the optimum compass performance so that there would be no evolutionary pressure to prolong relaxation times beyond this point (55, 56). Since the spike only emerges when the coherence time exceeds 1 μs, its presence could explain why slow relaxation might have evolved. Moreover, it may now become possible to understand how radiofrequency fields, in particular broadband anthropogenic electromagnetic noise (sometimes called electrosmog) (52), interferes with the operation of the avian compass – not because all anisotropy is destroyed (21) but because the spike is attenuated. It remains to be seen, however, whether the spin relaxation can be slow enough to explain the reported effects (52).

Experimental evidence. How could one determine whether a spike is really responsible for the precision of the avian magnetic compass? Although direct detection might be challenging, it should be possible to discover whether conditions could exist in a cryptochrome that would be compatible with the existence of a spike. Once it has been established which of the four known avian cryptochromes (13) plays a role in compass magnetoreception, and its structure is known, it will be possible to determine more about the librational motions of the radicals and the spin relaxation they produce. It seems probable that the magnetic and dynamic properties of a cryptochrome that has evolved as a compass sensor would differ significantly from those of cryptochromes that do not have a magnetic sensing function. It also appears likely that the properties of such a protein *in vivo* will differ from those of the isolated protein *in vitro*, for example as a result of binding to signalling partners or attachment to whatever intracellular structures are responsible for alignment and/or immobilization of the protein (28).

Another approach would be to extend the behavioural experiments mentioned above in which broadband sub-nanotesla electromagnetic noise was found to prevent European robins from using their magnetic compass (52). If, for example, the birds' ability to orient was disrupted by 1–100 kHz but by not 1–10 kHz broadband noise, this would provide evidence for radical pair lifetimes and spin relaxation times in the range 10–100 μs (50).

Quantum biology. The radical pair mechanism of magnetoreception has found a place in the emerging field of Quantum Biology (57-59) on the strength of the absolute requirement that the radical pair must be in a coherent superposition of the quantum states of the two electron spins. In fact, the initial electronic singlet state of the radical pair is quantum mechanically *entangled* (although the entanglement, as such, confers no advantage in terms of the general operation of the compass (60) and nor is it essential for the existence of the spike). We have recently shown that the spin dynamics of long-lived radical pairs in weak magnetic fields can be described by a semiclassical approximation that becomes increasingly accurate as the number of nuclear spins is increased (61, 62). If the behaviour of a realistic radical pair magnetoreceptor can be satisfactorily modelled in terms of classical rather than quantum oscillations, then arguably it does not belong under the quantum biological umbrella. However, the spike discussed here is undeniably a quantum effect, arising from the mixing of states associated with avoided energy-level crossings, and is not captured by the semiclassical theory. In this sense, radical pair magnetoreception may be more of a quantum phenomenon than hitherto realised.

Acknowledgements

This work was supported by the European Research Council (under the European Union's 7th Framework Programme, FP7/2007-2013/ERC grant agreement no. 340451), the Air Force Office of Scientific Research (Air Force Materiel Command, USAF award no. FA9550-14-1-0095), the EMF Biological Research Trust, the Deutsche Forschungsgemeinschaft (GRK 1885) and the Volkswagenstiftung (Lichtenberg Professur). P.J.H. thanks Malcolm Levitt and Stefan Weber for helpful discussions. We are grateful to Ilia Solov'yov for comments on the manuscript.

References

1. Wiltschko W, Munro U, Ford H, & Wiltschko R (1993) Red-light disrupts magnetic orientation of migratory birds. *Nature* 364(6437):525-527.
2. Mouritsen H, Feenders G, Liedvogel M, Wada K, & Jarvis ED (2005) Night-vision brain area in migratory songbirds. *Proc. Natl. Acad. Sci. USA* 102(23):8339-8344.
3. Zapka M*, et al.* (2009) Visual but not trigeminal mediation of magnetic compass information in a migratory bird. *Nature* 461(7268):1274-1278.
4. Mouritsen H & Hore PJ (2012) The magnetic retina: light-dependent and trigeminal magnetoreception in migratory birds. *Curr. Opin. Neurobiol.* 22:343-352.
5. Heyers D, Manns M, Luksch H, Gűntűrkűn O, & Mouritsen H (2007) A visual pathway links brain structures active during magnetic compass orientation in migratory birds. *Plos One* 2:e937.
6. Hein CM*, et al.* (2010) Night-migratory garden warblers can orient with their magnetic compass using the left, the right or both eyes. *J. Roy. Soc. Interface* 7:S227-S233.
7. Hein CM, Engels S, Kishkinev D, & Mouritsen H (2011) Robins have a magnetic compass in both eyes. *Nature* 471(7340):E11-E12.
8. Schulten K, Swenberg CE, & Weller A (1978) A biomagnetic sensory mechanism based on magnetic field modulated coherent electron spin motion. *Z. Phys. Chem. NF* 111:1-5.
9. Ritz T, Adem S, & Schulten K (2000) A model for photoreceptor-based magnetoreception in birds. *Biophys. J.* 78(2):707-718.
10. Cintolesi F, Ritz T, Kay CWM, Timmel CR, & Hore PJ (2003) Anisotropic recombination of an immobilized photoinduced radical pair in a 50-μT magnetic field: a model avian photomagnetoreceptor. *Chem. Phys.* 294(3):385-399.
11. Mouritsen H*, et al.* (2004) Cryptochromes and neuronal-activity markers colocalize in the retina of migratory birds during magnetic orientation. *Proc. Natl. Acad. Sci. USA* 101(39):14294-14299.
12. Rodgers CT & Hore PJ (2009) Chemical magnetoreception in birds: a radical pair mechanism. *Proc. Natl. Acad. Sci. USA* 106:353-360.
13. Liedvogel M & Mouritsen H (2010) Cryptochromes—a potential magnetoreceptor: what do we know and what do we want to know? *J. Roy. Soc. Interface* 7:S147-S162.
14. Niessner C*, et al.* (2011) Avian ultraviolet/violet cones identified as probable magnetoreceptors. *Plos One* 6(5):e20091.
15. Maeda K*, et al.* (2012) Magnetically sensitive light-induced reactions in cryptochrome are consistent with its proposed role as a magnetoreceptor. *Proc. Natl. Acad. Sci. USA* 109(13):4774-4779.
16. Lee AA*, et al.* (2014) Alternative radical pairs for cryptochrome-based magnetoreception. *J. Roy. Soc. Interface* 11:20131063.
17. Solov'yov IA, Chandler DE, & Schulten K (2007) Magnetic field effects in *Arabidopsis thaliana* cryptochrome-1. *Biophys. J.* 92(8):2711-2726.
18. Ludemann G, Solov'yov IA, Kubar T, & Elstner M (2015) Solvent driving force ensures fast formation of a persistent and well-separated radical pair in plant cryptochrome. *J. Amer. Chem. Soc.* 137(3):1147-1156.
19. Lau JCS, Rodgers CT, & Hore PJ (2012) Compass magnetoreception in birds arising from photo-induced radical pairs in rotationally disordered cryptochromes. *J. Roy. Soc. Interface* 9:3329-3337.
20. Cai J, Guerreschi GG, & Briegel HJ (2010) Quantum control and entanglement in a chemical compass. *Phys. Rev. Lett.* 104:220502.
21. Gauger EM, Rieper E, Morton JJL, Benjamin SC, & Vedral V (2011) Sustained quantum coherence and entanglement in the avian compass. *Phys. Rev. Lett.* 106(4):040503.

22. Bandyopadhyay JN, Paterek T, & Kaszlikowski D (2012) Quantum coherence and sensitivity of avian magnetoreception. *Phys. Rev. Lett.* 109(11):110502.
23. Dellis AT & Kominis IK (2012) The quantum Zeno effect immunizes the avian compass against the deleterious effects of exchange and dipolar interactions. *BioSyst.* 107(3):153-157.
24. Pauls JA, Zhang YT, Berman GP, & Kais S (2013) Quantum coherence and entanglement in the avian compass. *Phys. Rev. E* 87(6):062704.
25. Zhang YT, Berman GP, & Kais S (2014) Sensitivity and entanglement in the avian chemical compass. *Phys. Rev. E* 90(4):042707.
26. Xu BM, Zou J, Li H, Li JG, & Shao B (2014) Effect of radio frequency fields on the radical pair magnetoreception model. *Phys. Rev. E* 90(4):042711.
27. Carrillo A, Cornelio MF, & de Oliveira MC (2015) Environment-induced anisotropy and sensitivity of the radical pair mechanism in the avian compass. *Phys. Rev. E* 92(1):012720.
28. Solov'yov IA, Mouritsen H, & Schulten K (2010) Acuity of a cryptochrome and vision-based magnetoreception system in birds. *Biophys. J.* 99(1):40-49.
29. Wiltschko W & Wiltschko R (1972) Magnetic compass of European robins. *Science* 176(4030):62-64.
30. Gill RE*, et al.* (2009) Extreme endurance flights by landbirds crossing the Pacific Ocean: ecological corridor rather than barrier? *Proceedings of the Royal Society B-Biological Sciences* 276(1656):447-458.
31. Cochran WW, Mouritsen H, & Wikelski M (2004) Migrating songbirds recalibrate their magnetic compass daily from twilight cues. *Science* 304(5669):405-408.
32. Akesson S, Morin J, Muheim R, & Ottosson U (2001) Avian orientation at steep angles of inclination: experiments with migratory white-crowned sparrows at the magnetic North Pole. *Proc. Roy. Soc. B* 268(1479):1907-1913.
33. Lefeldt N, Dreyer D, Schneider NL, Steenken F, & Mouritsen H (2015) Migratory blackcaps tested in Emlen funnels can orient at 85 degrees but not at 88 degrees magnetic inclination. *J. Exp. Biol.* 218(2):206-211.
34. Timmel CR, Cintolesi F, Brocklehurst B, & Hore PJ (2001) Model calculations of magnetic field effects on the recombination reactions of radicals with anisotropic hyperfine interactions. *Chem. Phys. Lett.* 334(4,5,6):387-395.
35. Lau JCS, Wagner-Rundell N, Rodgers CT, Green NJB, & Hore PJ (2010) Effects of disorder and motion in a radical pair magnetoreceptor. *J. Roy. Soc. Interface* 7:S257-S264.
36. Timmel CR, Till U, Brocklehurst B, McLauchlan KA, & Hore PJ (1998) Effects of weak magnetic fields on free radical recombination reactions. *Mol. Phys.* 95(1):71-89.
37. Till U, Timmel CR, Brocklehurst B, & Hore PJ (1998) The influence of very small magnetic fields on radical recombination reactions in the limit of slow recombination. *Chem. Phys. Lett.* 298(1-3):7-14.
38. Efimova O & Hore PJ (2008) Role of exchange and dipolar interactions in the radical pair model of the avian magnetic compass. *Biophys. J.* 94(5):1565-1574.
39. Giovani B, Byrdin M, Ahmad M, & Brettel K (2003) Light-induced electron transfer in a cryptochrome blue-light photoreceptor. *Nat. Struct. Biol.* 10(6):489-490.
40. Zeugner A*, et al.* (2005) Light-induced electron transfer in *Arabidopsis* cryptochrome-1 correlates with *in vivo* function. *J. Biol. Chem.* 280(20):19437-19440.
41. Biskup T*, et al.* (2009) Direct observation of a photoinduced radical pair in a cryptochrome blue-light photoreceptor. *Angew. Chem. Internat. Ed.* 48(2):404-407.
42. Zoltowski BD*, et al.* (2011) Structure of full-length *Drosophila* cryptochrome. *Nature* 480(7377):396-399.
43. Levy C*, et al.* (2013) Updated structure of *Drosophila* cryptochrome. *Nature* 495:E3-E4.
44. Cai J, Caruso F, & Plenio MB (2012) Quantum limits for the magnetic sensitivity of a chemical compass. *Phys. Rev. A* 85(4):040304.
45. Hore PJ (2015) *Nuclear magnetic resonance* (Oxford University Press, Oxford).

46. Weaver JC, Vaughan TE, & Astumian RD (2000) Biological sensing of small field differences by magnetically sensitive chemical reactions. *Nature* 405(6787):707-709.
47. Rodgers CT (2007) Magnetic field effects in chemical systems. D. Phil. thesis, University of Oxford.
48. Hogben HJ, Efimova O, Wagner-Rundell N, Timmel CR, & Hore PJ (2009) Possible involvement of superoxide and dioxygen with cryptochrome in avian magnetoreception: origin of Zeeman resonances observed by *in vivo* EPR spectroscopy. *Chem. Phys. Lett.* 480:118-122.
49. Solov'yov IA & Schulten K (2009) Magnetoreception through cryptochrome may involve superoxide. *Biophys. J.* 96:4804-4813.
50. Ritz T*, et al.* (2009) Magnetic compass of birds is based on a molecule with optimal directional sensitivity. *Biophys. J.* 96:3451-3457.
51. Schwarze S*, et al.* (2016) Weak broadband electromagnetic fields are more disruptive to magnetic compass orientation in a night-migratory songbird (*Erithacus rubecula*) than strong narrow-band fields. *Front. Behav. Neurosci.*:doi: 10.3389/fnbeh.2016.00055.
52. Engels S*, et al.* (2014) Anthropogenic electromagnetic noise disrupts magnetic compass orientation in a migratory bird. *Nature* 509(7500):353-356.
53. Kavokin KV (2009) The puzzle of magnetic resonance effect on the magnetic compass of migratory birds. *Bioelectromagnetics* 30(5):402-410.
54. Gauger EM & Benjamin SC (2013) Comment on "Quantum coherence and sensitivity of avian magnetoreception". *Phys. Rev. Lett.* 110(17):178901.
55. Stoneham AM, Gauger EM, Porfyrakis K, Benjamin SC, & Lovett BW (2012) A new type of radical-pair-based model for magnetoreception. *Biophys. J.* 102(5):961-968.
56. Lambert N, De Liberato S, Emary C, & Nori F (2013) Radical-pair model of magnetoreception with spin-orbit coupling. *New J. Phys.* 15:083024.
57. Ball P (2011) Physics of life: the dawn of quantum biology. *Nature* 474:272-274.
58. Al-Khalili J & McFadden J (2014) *Life on the edge: the coming of age of quantum biology* (Bantam Press, London).
59. Solov'yov IA, Ritz T, Schulten K, & Hore PJ (2014) A chemical compass for bird navigation. *Quantum Effects in Biology*, eds Mohseni M, Omar Y, Engel GS, & Plenio MB (Cambridge University Press, Cambridge), pp 218-236.
60. Hogben HJ, Biskup T, & Hore PJ (2012) Entanglement and sources of magnetic anisotropy in radical pair-based avian magnetoreceptors. *Phys. Rev. Lett.* 109:220501.
61. Manolopoulos DE & Hore PJ (2013) An improved semiclassical theory of radical pair recombination reactions. *J. Chem. Phys.* 139:124106.
62. Lewis AM, Manolopoulos DE, & Hore PJ (2014) Asymmetric recombination and electron spin relaxation in the semiclassical theory of radical pair reactions. *J. Chem. Phys.* 141(4):044111.

Figure captions

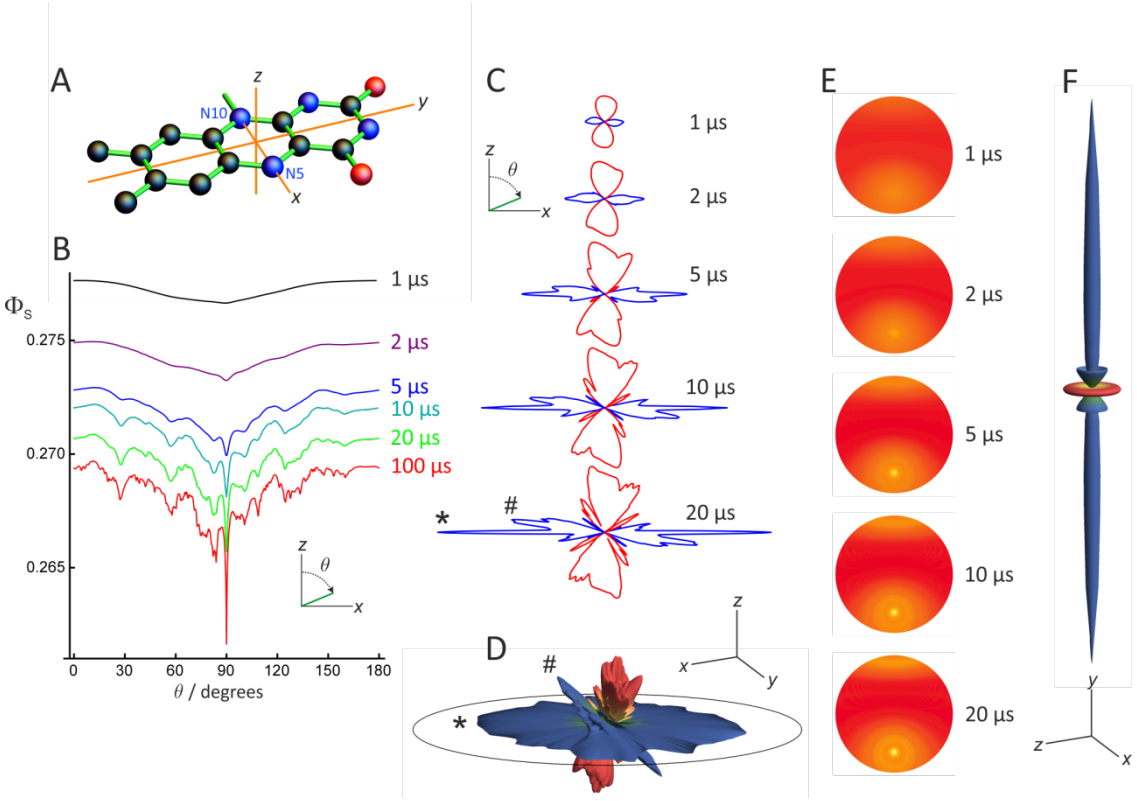

Fig. 1. Reaction yields of a [$FAD^{\bullet-}$ $TrpH^{\bullet+}$] radical pair.

A. The axis system used in the simulations superimposed on the tricyclic flavin ring system.

B. The variation of Φ_S with θ for radical pairs with lifetimes between 1 µs and 100 µs. For clarity, two of the traces have been offset vertically: by –0.001 (light green) and –0.002 (red). θ specifies the direction of the magnetic field in the *zx*-plane of the flavin.

C. The same data as in B (1–20 µs lifetimes) presented as two-dimensional polar plots. In each case, only the anisotropic part of Φ_S is shown, with red and blue indicating values respectively larger and smaller than the isotropic value. The five plots are drawn on the same scale. The blue features at $\theta = \pm 90°$ (labelled $*$ in the 20 µs plot) are the spikes.

D. The anisotropic part of Φ_S (10 µs lifetime) presented as a three-dimensional polar plot. A circle in the *xy*-plane ($\theta = 90°$) is included as a guide to the eye. The blue disk in the *xy*-plane (labelled $*$) gives rise to the spike. The smaller blue disk, labelled # (also in C), angled at approximately 40° to the *xy*-plane, comes principally from the N1 indole nitrogen of $TrpH^{\bullet+}$. Its tilt reflects the orientation of the indole group of the tryptophan relative to the flavin (42, 43).

E. Visual modulation patterns calculated from Φ_S (1–20 µs lifetimes) representing the directional information available from an array of cryptochrome-containing magnetoreceptor cells distributed around the retina. The bright spot in the lower half of the pattern arises from the spike.

F. Three-dimensional polar plot of Φ_S (10 µs lifetime) averaged over a 360° rotation around an axis in the *xy*-plane. This object has been rotated by 90° relative to D and scaled up by a factor of 2.1. The patterns in E were calculated using the same averaging procedure (SI Appendix, Section S6).

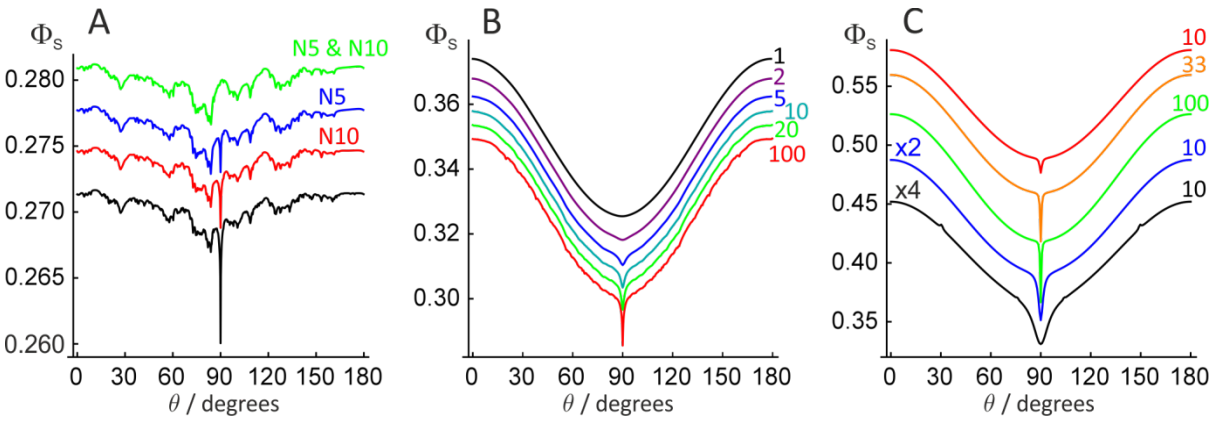

Fig. 2. Reaction yields of various radical pairs.

A. Φ_S for a [$FAD^{\bullet-}$ $TrpH^{\bullet+}$] radical pair in which the transverse principal components of selected nitrogen hyperfine interactions (A_{xx} and A_{yy}) were set to zero: for N5 (blue), N10 (red), and both N5 and N10 (green). Φ_S for the unmodified [$FAD^{\bullet-}$ $TrpH^{\bullet+}$] is shown in black. In all cases, τ = 1 ms. For clarity, three of the traces have been offset vertically: by 0.006 (green) and 0.003 (blue and red).

B. Φ_S for a [$FAD^{\bullet-}$ $Y^{\bullet}$] radical pair in which radical $Y^{\bullet}$ contains a single ^{14}N nucleus with an axial hyperfine tensor with principal components (A_{xx}, A_{yy}, A_{zz}) = (0.0, 0.0, 1.0812) mT (modelled on N1 in $TrpH^{\bullet+}$). The radical pair lifetimes are as indicated (1–100 μs). The angle between the *z*-axes of $Y^{\bullet}$ and $FAD^{\bullet-}$ was 45°; the intensity of the spike was found to decrease smoothly to zero as this angle was increased from zero to 90°. For clarity, the five traces for τ < 100 μs have been offset vertically, from top to bottom, by 0.020, 0.016, 0.012, 0.008, and 0.004 respectively.

C. Φ_S for toy radical pairs, [$X^{\bullet}$ $Y^{\bullet}$]. For the red, orange and green traces, $X^{\bullet}$ contains a single ^{14}N hyperfine tensor with principal components (A_{xx}, A_{yy}, A_{zz}) = (–0.0989, –0.0989, 1.7569) mT. For the blue and black traces, (A_{xx}, A_{yy}, A_{zz}) = (–0.2, –0.2, 1.7569) mT and (–0.4, –0.4, 1.7569) mT, respectively. In all five cases $Y^{\bullet}$ contains a single ^{14}N nucleus with an axial hyperfine interaction: (A_{xx}, A_{yy}, A_{zz}) = (0.0, 0.0, 1.0812) mT. The two hyperfine tensors have parallel *z*-axes. The radical pair lifetimes are as indicated (10, 33.3, 100 μs). ×2 and ×4 indicate the doubling and quadrupling of A_{xx} and A_{yy} in $X^{\bullet}$. For clarity, three of the traces have been offset vertically: by 0.03 (green), 0.06 (orange and red).

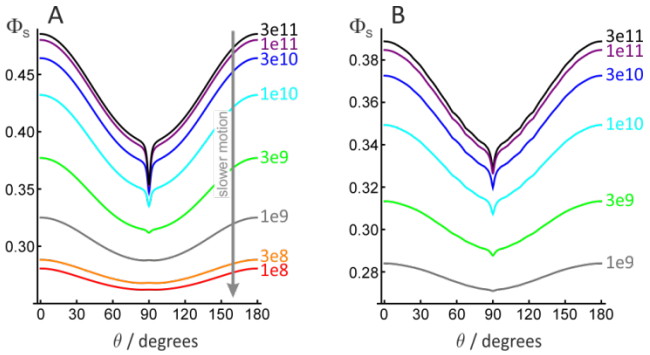

Fig. 3. Reaction yields of radical pairs with spin relaxation included.

A. The toy radical pair, [$X^{\bullet}$ $Y^{\bullet}$]. $X^{\bullet}$ has a single ^{14}N nucleus with hyperfine components (A_{xx}, A_{yy}, A_{zz}) = (–0.2, –0.2, 1.7569) mT; $Y^{\bullet}$ has a single ^{14}N nucleus with hyperfine components (0.0, 0.0, 1.0812) mT. The two hyperfine tensors have parallel *z*-axes. The radical pair lifetime is 10 μs. $X^{\bullet}$ underwent 10° rotational jumps (i.e. β = 5°) around the *y*-axis with rate constants k_r between $3 \times 10^{11}\,s^{-1}$ and $10^{8}\,s^{-1}$, as indicated.

B. The [$FAD^{\bullet-}$ $Y^{\bullet}$] radical pair. $FAD^{\bullet-}$ has seven magnetic nuclei, as in Fig. 1. $Y^{\bullet}$ has single ^{14}N nucleus with hyperfine components (A_{xx}, A_{yy}, A_{zz}) = (0.0, 0.0, 1.0812) mT. The radical pair lifetime is 10 μs. $FAD^{\bullet-}$ underwent 10° rotational jumps (i.e. β = 5°) around the *y*-axis with rate constants k_r varying between $3 \times 10^{11}\,s^{-1}$ and $10^{9}\,s^{-1}$, as indicated. In both A and B, the direction of the magnetic field (θ) is varied in the *zx*-plane of the flavin ring system (Fig. 1A). Almost identical results were found for the *zy*-plane.

The quantum needle of the avian magnetic compass

Hamish G. Hiscock, Susannah Worster, Daniel R. Kattnig, Charlotte Steers, Ye Jin, David E. Manolopoulos, Henrik Mouritsen and P. J. Hore*

* To whom correspondence may be addressed: peter.hore@chem.ox.ac.uk

Supporting Information

S1. Hyperfine interactions and relative orientation of $FAD^{\bullet-}$ *and* $TrpH^{\bullet+}$

Table S1. Hyperfine tensors for the $FAD^{\bullet-}$ radical.♥

Nucleus	A	a_{iso}/mT♦	T_{qq}/mT ♣
N5	$\begin{pmatrix} -0.0989 & 0.0039 & 0.0 \\ 0.0039 & -0.0881 & 0.0 \\ 0.0 & 0.0 & 1.7569 \end{pmatrix}$	0.5233	1.2336 –0.6101 –0.6234
N10	$\begin{pmatrix} -0.0190 & -0.0048 & 0.0 \\ -0.0048 & -0.0196 & 0.0 \\ 0.0 & 0.0 & 0.6046 \end{pmatrix}$	0.1887	0.4159 –0.2031 –0.2128
H6	$\begin{pmatrix} -0.2569 & -0.1273 & 0.0 \\ -0.1273 & -0.4711 & 0.0 \\ 0.0 & 0.0 & -0.4336 \end{pmatrix}$	–0.3872	0.1896 –0.0464 –0.1432
H8 (×3)	$\begin{pmatrix} 0.4399 & 0.0 & 0.0 \\ 0.0 & 0.4399 & 0.0 \\ 0.0 & 0.0 & 0.4399 \end{pmatrix}$	0.4399	0.0 0.0 0.0
Hβ (×2)	$\begin{pmatrix} 0.4070 & 0.0 & 0.0 \\ 0.0 & 0.4070 & 0.0 \\ 0.0 & 0.0 & 0.4070 \end{pmatrix}$	0.4070	0.0 0.0 0.0
H7 (×3)	$\begin{pmatrix} -0.1416 & 0.0 & 0.0 \\ 0.0 & -0.1416 & 0.0 \\ 0.0 & 0.0 & -0.1416 \end{pmatrix}$	–0.1416	0.0 0.0 0.0

♥Calculated by Dr Ilya Kuprov, Department of Chemistry, University of Southampton using density functional theory in Gaussian-03 (1) at the UB3LYP/EPR-III level (2). The calculation was done for the radical anion of 7,8,10-trimethyl isoalloxazine (lumiflavin) *in vacuo*. The atom numbering scheme is shown below.

♦Isotropic hyperfine interactions.

♣Principal anisotropic components of the hyperfine tensors (arranged in descending order of magnitude for each nucleus).

Notes:

H8 methyl group. The anisotropic components are small (< 0.08 mT) and were not included in the spin dynamics simulations. The average of the three isotropic couplings, (0.6493 + 0.6493 + 0.0212)/3 mT, was used for all three methyl protons on the assumption that methyl group rotation is fast enough to average the three interactions.

H7 methyl group. The anisotropic components are small (< 0.05 mT) and were not included in the spin dynamics simulations. The average of the three isotropic couplings, −(0.2011 + 0.2011 + 0.0225)/3 mT, was used for all three methyl protons on the assumption that methyl group rotation is fast enough to average the three interactions.

Hβ. The anisotropic components are small (< 0.09 mT) and were not included. The β protons were assigned isotropic hyperfine couplings equal to the largest of the three calculated for the N(10) methyl group in lumiflavin (0.4070, 0.4070, −0.0189 mT).

Choice of nuclei. The spin dynamics calculations reported in the main text included the following 7 nuclei: N5, N10, H6, 3×H8, 1×Hβ.

The *DFT calculations* were performed separately for the two radicals on the assumption that the 1.9 nm centre-to-centre distance between them in the protein is large enough that the hyperfine interactions should be very similar in the radical pair.

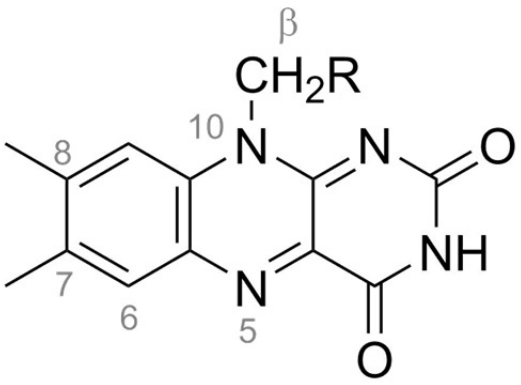

Table S2. Hyperfine tensors for the $TrpH^{\bullet+}$ radical.♥

Nucleus	**A** ♠	a_{iso}/mT♦	T_{qq}/mT ♣
N1	$\begin{pmatrix} -0.0336 & 0.0924 & -0.1354 \\ 0.0924 & 0.3303 & -0.5318 \\ -0.1354 & -0.5318 & 0.6680 \end{pmatrix}$	0.3215	0.7596 −0.3745 −0.3851
H1	$\begin{pmatrix} -0.9920 & -0.2091 & -0.2003 \\ -0.2091 & -0.2631 & 0.2803 \\ -0.2003 & 0.2803 & -0.5398 \end{pmatrix}$	−0.5983	0.5914 −0.1071 −0.4843
H2	$\begin{pmatrix} -0.2843 & 0.1757 & 0.1525 \\ 0.1757 & -0.2798 & 0.0975 \\ 0.1525 & 0.0975 & -0.2699 \end{pmatrix}$	−0.2780	0.2855 −0.0919 −0.1936
H4	$\begin{pmatrix} -0.5596 & -0.1956 & -0.1657 \\ -0.1956 & -0.4020 & 0.0762 \\ -0.1657 & 0.0762 & -0.5021 \end{pmatrix}$	−0.4880	0.3001 −0.0480 −0.2520
H6	$\begin{pmatrix} -0.0506 & 0.0622 & 0.0889 \\ 0.0622 & -0.3100 & -0.0297 \\ 0.0889 & -0.0297 & 0.2642 \end{pmatrix}$	−0.2083	0.1979 −0.0494 −0.1485
H7	$\begin{pmatrix} -0.4355 & -0.1541 & -0.1239 \\ -0.1541 & -0.2777 & 0.0864 \\ -0.1239 & 0.0864 & -0.3770 \end{pmatrix}$	−0.3636	0.2540 −0.0594 −0.1945
Hβ1	$\begin{pmatrix} 1.5808 & -0.0453 & -0.0506 \\ -0.0453 & 1.5575 & 0.0988 \\ -0.0506 & 0.0988 & 1.6752 \end{pmatrix}$	1.6046	0.1521 −0.0456 −0.1065
Hα	$\begin{pmatrix} -0.0601 & 0.0037 & 0.0331 \\ 0.0037 & -0.0251 & 0.0111 \\ 0.0331 & 0.0111 & -0.1940 \end{pmatrix}$	−0.0931	−0.1092 0.0395 0.0698
N*	$\begin{pmatrix} 0.1295 & -0.0134 & 0.0075 \\ -0.0134 & 0.1729 & -0.0249 \\ 0.0075 & -0.0249 & 0.1371 \end{pmatrix}$	0.1465	−0.0224 −0.0207 0.0431

Hβ2	$\begin{pmatrix} 0.1634 & -0.0230 & -0.0064 \\ -0.0230 & -0.0082 & 0.0158 \\ -0.0064 & 0.0158 & -0.0182 \end{pmatrix}$	0.0457	–0.0758 –0.0454 0.1211
H5	$\begin{pmatrix} 0.0051 & 0.0616 & 0.0694 \\ 0.0616 & -0.0665 & 0.0391 \\ 0.0694 & 0.0391 & -0.0586 \end{pmatrix}$	–0.0400	–0.0632 –0.0616 0.1248

♥Calculated by Dr Ilya Kuprov, Department of Chemistry, University of Southampton using density functional theory in Gaussian-03 (1) at the UB3LYP/EPR-III level (2). The calculation was done for the radical cation of tryptophan *in vacuo*. The atom numbering scheme is shown below.

♠Full hyperfine tensors in the same axis system as $FAD^{\bullet-}$ (Table S1). The relative orientation of the two radicals was taken to be that of the FAD cofactor and Trp-342 (the terminal tryptophan of the Trp-triad) in the crystal structure of *Drosophila melanogaster* cryptochrome (*Dm*Cry, PDB entry 4GU5 (3, 4)).

♦Isotropic hyperfine interactions.

♣Principal anisotropic components of the hyperfine tensors (arranged in descending order of magnitude for each nucleus).

*The nitrogen of the NH_2 group.

Notes:

Choice of nuclei. The spin dynamics calculations reported in the main text included the following 7 nuclei: N1,H1, H2, H4, H5, H7, Hβ1.

The DFT calculations were performed separately for the two radicals on the assumption that the 1.9 nm centre-to-centre distance between them in the protein is large enough that the hyperfine interactions should be very similar in the radical pair.

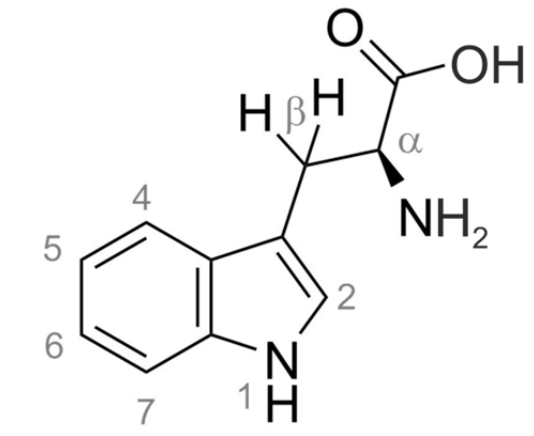

The relative orientation of the two radicals was taken to be that of FAD and Trp-342 in *Drosophila melanogaster* cryptochrome (PDB entry 4GU5, A chain) (3, 4) and is depicted below.

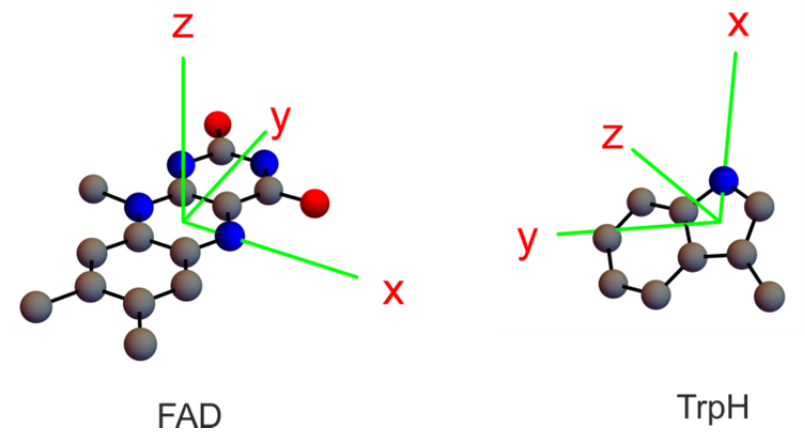

In each radical, the *z*-axis is the normal to the plane of the aromatic ring system. The angle between the two *z*-axes is 39.2°. The rotation matrix that maps the (*x*, *y*, *z*) axes of the tryptophan indole group onto those of the FAD isoalloxazine group is:

$$R = \begin{pmatrix} -0.3454 & 0.6869 & -0.6395 \\ -0.8269 & 0.0995 & 0.5535 \\ 0.4438 & 0.7199 & 0.5336 \end{pmatrix}.$$

S2. [FAD$^{\bullet-}$ TrpH$^{\bullet+}$] simulations with ≥14 nuclear spins included

Fig. S1 shows the effect on the reaction yield anisotropy of increasing the number of nuclear spins, *N*, included in the calculation (cf. *N* = 14 in Fig. 1C in the main text). The five polar plots are drawn on the same scale. The *N*/2 nuclear spins in each radical were taken in order (left to right) from Table S3. The hyperfine tensors are given in Section S1.

Although the spike is somewhat attenuated by the extra nuclei, it is relatively much less affected than the broad background signal.

Table S3. Nuclei included in the calculations.

FAD$^{\bullet-}$	N5	N10	H6	H8	H8	H8	Hβ	Hβ	H7	H7	H7
TrpH$^{\bullet+}$	N1	H1	H2	H4	H6	H7	Hβ1	Hα	N*	Hβ2	H5

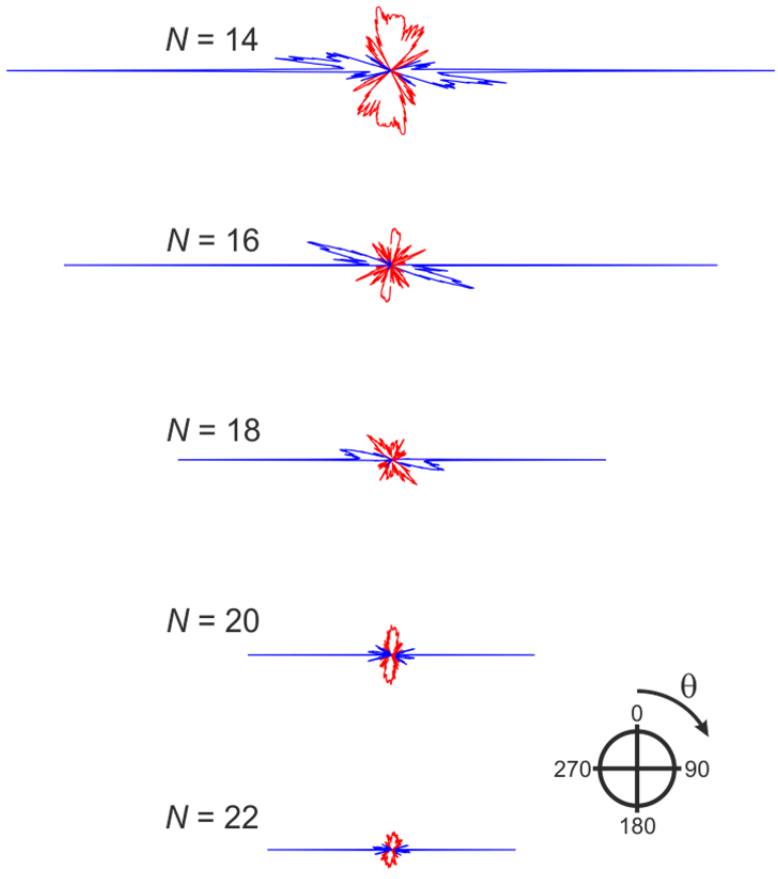

Fig. S1. Two-dimensional polar plots of the anisotropic part of Φ_S (as in Fig. 1C). Red and blue indicate values respectively larger and smaller than the isotropic value.

S3. Asymmetric recombination kinetics

The calculations presented in the main text were all performed for a reaction scheme in which singlet and triplet radical pairs recombined spin-selectively with identical rate constants ($k_S = k_T = k = \tau^{-1}$) to form distinct products. Calculations, shown in Fig. S2, performed for the toy radical pair [$X^\bullet$ $Y^\bullet$] (with one ^{14}N hyperfine interaction in each radical – as in Fig. 2C) show that the spike at $\theta = 90°$ persists even when the two rate constants differ by an order of magnitude.

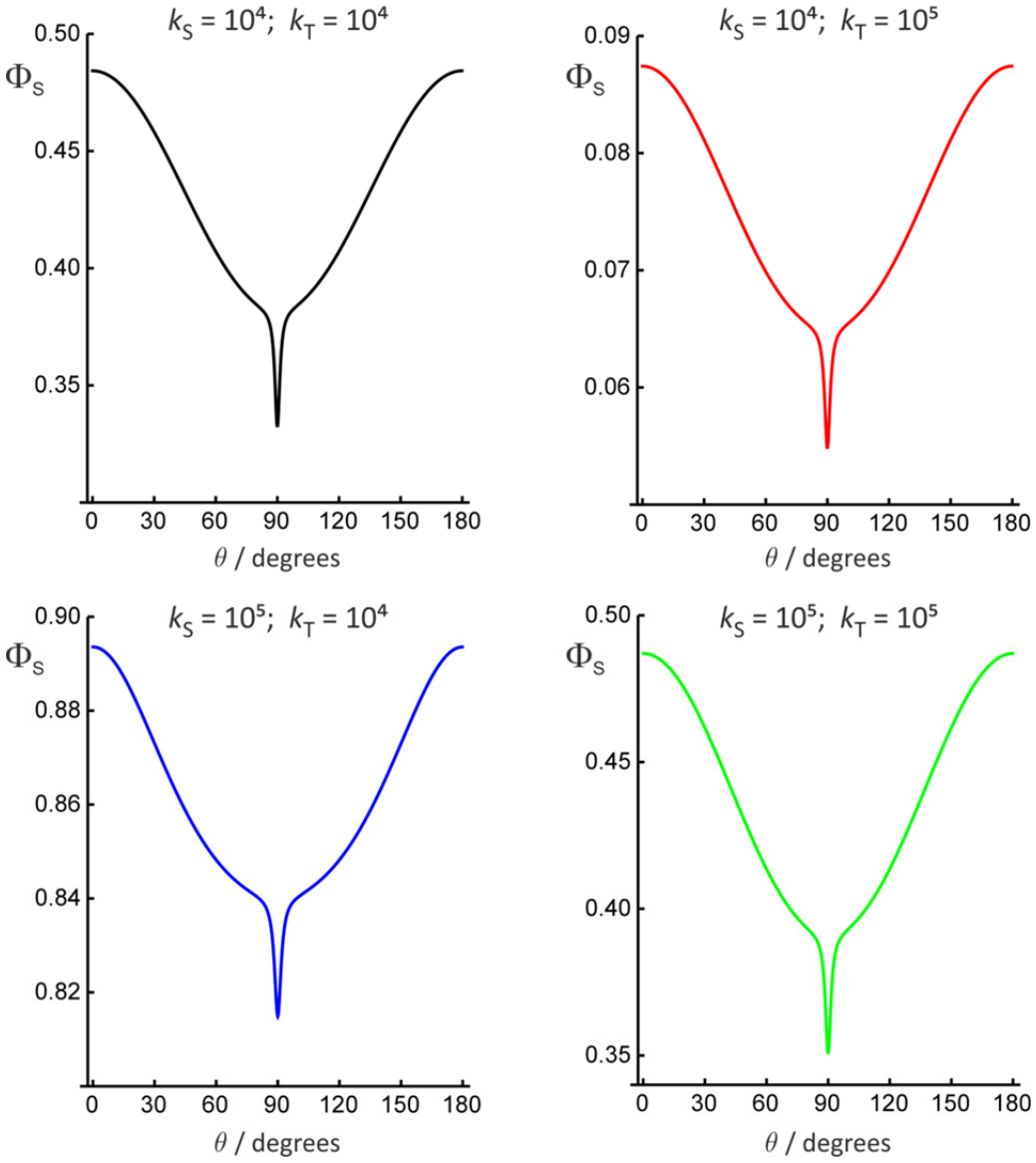

Fig. S2. Φ_S for a toy radical pair, [$X^\bullet$ $Y^\bullet$]. $X^\bullet$ contains a single ^{14}N hyperfine tensor with principal components (A_{xx}, A_{yy}, A_{zz}) = (–0.0989, –0.0989, 1.7569) mT (based on N5 in $FAD^{\bullet-}$). $Y^\bullet$ contains a single ^{14}N nucleus with (A_{xx}, A_{yy}, A_{zz}) = (0.0, 0.0, 1.0812) mT (based on N1 in $TrpH^{\bullet+}$). The two hyperfine tensors have parallel *z*-axes. The singlet and triplet recombination rate constants (s^{-1}) are as indicated.

S4. Exchange and dipolar interactions

Preliminary simulations using the toy radical pair model suggest that the spike can be affected by the exchange and dipolar interactions of the electron spins in the two radicals. These effects are probably less pronounced for radicals with many nuclear spins but this is difficult to verify because the Liouville-space calculations required when electron-electron interactions are included become prohibitively slow for realistic spin systems. The effects of spin-spin interactions may also be reduced by the partial cancellation of the exchange and dipolar contributions predicted for a radical pair with a separation close to that of $FAD^{\bullet-}$ and $TrpH^{\bullet+}$ in cryptochrome (5). Finally, if in a migratory bird cryptochrome, as in *Xenopus laevis* (6-4) photolyase (6), there are four instead of three Trp residues involved in photoreduction of the FAD, then the magnetically sensitive FAD-Trp radical pair could have a larger distance between the radical centres and consequently smaller spin-spin interactions.

S5. Calculation of Φ_S in the absence of molecular motion

Magnetic field effects were modelled by means of the following reaction scheme.

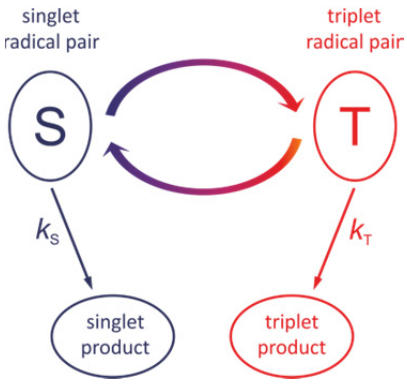

'Singlet' (S) and 'triplet' (T) refer to the states of the two electron spins, one in each radical. The curved arrows represent the coherent spin dynamics arising from the combined effects of Zeeman and hyperfine interactions. The straight arrows are spin-selective reaction steps. The radical pair is created in a singlet state by spin-conserving electron transfer. Singlet and triplet radical pairs are considered to undergo separate spin-conserving reverse electron transfer reactions to form distinct singlet and triplet products. Abstract examples of such reactions are $^{S}\left[A^{\bullet+}B^{\bullet-}\right] \rightarrow {}^{S}A + {}^{S}B$ and $^{T}\left[A^{\bullet+}B^{\bullet-}\right] \rightarrow {}^{T}A + {}^{S}B$ where ^{S}A and ^{S}B are diamagnetic (closed shell, singlet state) molecules with no unpaired electron spins and ^{T}A is a paramagnetic molecular triplet. In the model, the rate constants of these two reactions are identical: $k_S = k_T = k = 1/\tau$. We calculate Φ_S, the fractional yield of the singlet product once all radical pairs have reacted. Φ_S is related to the yield of the triplet product by $\Phi_T = 1 - \Phi_S$.

The singlet yield Φ_S was calculated as (7, 8):

$$\Phi_S = k\int_0^\infty p_S(t)\,\mathrm{e}^{-kt}\,\mathrm{d}t$$

in which $k = k_S = k_T$ is the recombination rate constant and $p_S(t)$ is the fraction of radical pairs in the singlet state at time t (9):

$$p_S(t) = \frac{1}{4} + \sum_{p=x,y,z}\sum_{q=x,y,z} R_{pq}^{(\mathrm{A})}(t)R_{pq}^{(\mathrm{B})}(t)$$

with

$$R_{pq}^{(m)}(t) = \frac{1}{Z_m}\mathrm{Tr}\left[\hat{S}_{mp}\mathrm{e}^{-\mathrm{i}\hat{H}_m t}\hat{S}_{mq}\mathrm{e}^{\mathrm{i}\hat{H}_m t}\right]$$

and

$$Z_m = \prod_{j=1}^{N_m}\left(2I_{mj}+1\right).$$

$\hat{S}_{mp}$ ($p = x,y,z$) are the electron spin operators and $\hat{H}_m$ is the spin Hamiltonian of radical m (m = A, B). I_{mj} is the spin quantum number of nucleus j in radical m and N_m is the number of nuclei in radical m.

The spin Hamiltonian for each radical contains terms for the Zeeman interaction (Z) of the electron spin with the applied magnetic field, and the various hyperfine interactions (HFI) in the two radicals:

$$\hat{H}_m = \hat{H}_{m,\mathrm{Z}}(\theta,\phi) + \hat{H}_{m,\mathrm{HFI}}$$

with

$$\hat{H}_{m,\mathrm{Z}}(\theta,\phi) = \gamma_{\mathrm{e}} B_0 \left[\hat{S}_{mx} \sin\theta\cos\phi + \hat{S}_{my} \sin\theta\sin\phi + \hat{S}_{mz} \cos\theta \right]$$

and

$$\hat{H}_{m,\mathrm{HFI}} = \sum_{j=1}^{N_m} \left[a_{mj}^{\mathrm{iso}} \hat{\mathbf{S}}_m \bullet \hat{\mathbf{I}}_{mj} + \hat{\mathbf{S}}_m \bullet \mathbf{T}_{mj} \bullet \hat{\mathbf{I}}_{mj} \right]$$

where B_0 is the strength of the external magnetic field, θ and ϕ define its direction with respect to the radical pair, a_{mj}^{iso} is the isotropic hyperfine coupling constant and $\mathbf{T}_{mj}$ is the anisotropic part of the hyperfine interaction tensor of nucleus j coupled to electron m. $\hat{\mathbf{I}}_{mj}$ is the nuclear spin operator of nucleus j coupled to electron m.

The main text summarizes the conditions under which the simulations were performed.

S6. Visual modulation patterns

"Visual modulation patterns", first calculated by Ritz *et al*. (10), are crude representations of a bird's perception of the compass information delivered by an array of cryptochrome-containing magnetoreceptor cells distributed around its retina. The proteins are assumed to be identically oriented in every cell and each cell to be identically oriented with respect to the local retina normal. Cells at different locations in the retina have different orientations with respect to the geomagnetic field and therefore deliver different directional information. The assumption is that either by comparing the signals from different parts of the retina or by performing head scans, or both, the bird would obtain information sufficient to orient itself. As noted by Ritz *et al*. (11), different arrangements of the cryptochromes, e.g. a perpendicular orientation of the proteins in neighbouring cells, can result in different sensitivity to the geomagnetic field. However, the clarity of the sensory information for these alternative arrangements would be similar to that of the simulations used here for illustrative purposes.

The visual modulation patterns for [$FAD^{\bullet-}$ $TrpH^{\bullet+}$] in Fig. 1E were calculated as described by Lau *et al*. (12). The cells were assumed to have no preferred orientation with respect to rotation around the local retina normal (13). This ordering is not unlike that of the rod and cone visual receptor cells in the retina (one of the proposed locations for cryptochrome magnetoreceptors (13, 14)). The signals were therefore integrated over the angle η (defined in the Electronic Supplementary Material of Ref. (12)). The *z*-axes of the FAD molecules within each cell were assumed to be perpendicular to this symmetry axis so that the η-averaging of Φ_S is around an axis in the *xy*-plane of the flavin ring system. Fig 1F was calculated from Fig. 1D using the same averaging.

Fig. S3 summarizes the geometry of the model and the various rotations. In the visual modulation patterns, θ varies from zero at the centre of the pattern to 90° at the edge. ϕ increases anticlockwise from zero at the bottom.

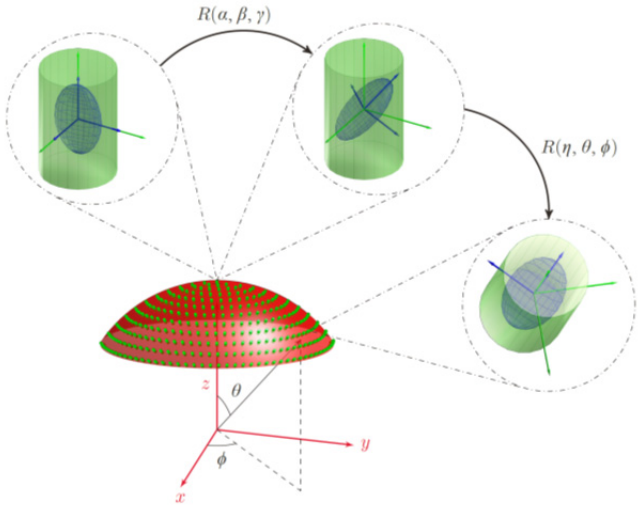

Fig. S3. Cells (green spots) are distributed around the retina (red dome). Euler angles (α,β,γ) define the orientation of cryptochrome molecules (blue) within each cell. Euler angles (η,θ,ϕ) define the position of the cell in the retina. η specifies the rotation of the cell around its *z*-axis, shown here as a cylindrical symmetry axis. Taken from Ref. (15).

S7. Hyperfine interactions of flavin radicals in proteins

Table S4 summarizes the available experimental measurements of the hyperfine tensor components of the N5 and N10 nitrogens in flavin radicals in proteins. Also included at the bottom of the Table are some DFT calculations of hyperfine interactions in a neutral flavin radical for comparison with those used in the present study. Additionally, Eriksson & Ehrenberg (16) reported $A_{xx} = A_{yy} = 0.25a_{\text{iso}}$ and $A_{zz} = 2.5a_{\text{iso}}$ for a flavin radical in *Azotobacter vinelandii* NADPH dehydrogenase.

All values are given in MHz. The principal components, A_{qq}, are related to the quantities in Table S1 by $A_{qq} = a_{\text{iso}} + T_{qq}$.

Although the values of A_{xx}, A_{yy}, and A_{zz} vary considerably, in all cases $A_{zz} > 10|A_{xx}|, 10|A_{yy}| \neq 0$, as required for the existence of a spike in Φ_S.

Table S4. Hyperfine tensor components of flavin radicals

protonation state of flavin	protein	reference		$A_{xx} = A_{yy}$ ♣	A_{zz} ♣
neutral	*Anabaena* flavodoxin	(17)	N10	3 ± 1	31 ± 1
neutral	*Anabaena* ferredoxin $NADP^+$ reductase	(18)	N10	2.7 ± 1.3	29.7 ± 1.9
neutral	Na^+ translocating NADH:quinone oxidoreductase *Vibrio cholerae*	(19)	N5	0.2 ± 2.0	52.5 ± 0.5
			N10	2.0 ± 1.0	28.9 ± 0.6
anionic	Na^+ translocating NADH:quinone oxidoreductase *Vibrio cholerae*	(19)	N5	2.3 ± 0.6	57.6 ± 0.5
			N10	1.6 ± 0.6	22.8 ± 0.6

protonation state of flavin	calculation	reference		$A_{xx} = A_{yy}$	A_{zz}
anionic	DFT UB3LYP/EPR-III	This work	N5	−2.6	49.2
			N10	−0.5	16.9
neutral ♥	DFT B3LYP/EPR-II	(20)	N5	−0.5	40.6
			N10	−0.8	19.3
neutral ♠	DFT B3LYP/EPR-II	(20)	N5	−1.7	42.7
			N10	0.9	23.1

♣The signs of the A_{qq} values were not determined.
♥$FADH^\bullet$ with the ribityl side chain truncated after the C3′ carbon.
♠$FADH^\bullet$ with the ribityl side chain truncated after the C3′ carbon, with amino acid fragments included to mimic the protein environment of FAD in *E. coli* DNA photolyase.

S8. Avoided energy-level crossings

We demonstrate here that the spike can be unambiguously attributed to avoided crossings of the quantum mechanical energy levels of the radical pair spin Hamiltonian as a function of the magnetic field direction.

In the case that singlet and triplet react to form separate products with the same rate constant k, Φ_S may be obtained from (7):

$$\Phi_S = \frac{1}{Z}\sum_m\sum_n \left|P^S_{mn}\right|^2 \frac{k^2}{k^2+\left(\omega_m-\omega_n\right)^2} \ . \tag{1}$$

Z is the total number of nuclear spin configurations and $\hat{P}^S$ is the singlet projection operator with matrix elements $P^S_{mn} = \langle m|\hat{P}^S|n\rangle$. $|n\rangle$ and $|m\rangle$ are eigenstates of the radical pair spin Hamiltonian, $\hat{H} = \hat{H}_A + \hat{H}_B$, with eigenvalues ω_n and ω_m respectively.

We consider two basis states, $|1\rangle$ and $|2\rangle$, with the following Hamiltonian matrix elements ($H_{jk} = \langle j|\hat{H}|k\rangle$):

$$H_{11} = +aq; \ \ H_{22} = -aq; \ \ H_{12} = H_{21} = b\,, \tag{2}$$

where the variable q defines the direction of the magnetic field relative to the radical pair. q corresponds to the angle $\theta - 90°$ in the main text. a plays the role of A_{zz} and the weak Zeeman interaction; b plays the role of $\sqrt{A_{xx}^2 + A_{yy}^2}$. The latter can be regarded as a small perturbation. The A_{zz} term together with the interaction of the electron spins with the external magnetic field causes the energy levels to vary approximately linearly in the neighbourhood of θ = 90° (hence the $\pm aq$ terms). A_{xx} and A_{yy} (the b term) couple the two states and lead to the avoided crossing when $\theta \approx 90°$.

Solving the secular equations for this two-level system gives the eigenvalues $\varepsilon_\pm$ and eigenvectors $|\pm\rangle$:

$$\varepsilon_\pm = \pm\sqrt{a^2q^2+b^2} \tag{3}$$

$$\begin{aligned} |+\rangle &= \cos\zeta|1\rangle + \sin\zeta|2\rangle \\ |-\rangle &= \sin\zeta|1\rangle - \cos\zeta|2\rangle \end{aligned}, \tag{4}$$

where

$$\tan 2\zeta = \frac{b}{aq}\,. \tag{5}$$

When $b = 0$, the energy levels cross at q = 0 ($\varepsilon_\pm = 0$); when $b \neq 0$, this becomes an avoided crossing ($\varepsilon_\pm = \pm b$). Assuming

$$P^S_{11} = p_1, \quad P^S_{22} = p_2, \quad P^S_{12} = P^S_{21} = 0 \tag{6}$$

i.e. that the basis states have different singlet characters (p_1 and p_2), one finds:

$$\begin{aligned} P^S_{++} &= \Sigma + \Delta\cos(2\zeta) \\ P^S_{--} &= \Sigma - \Delta\cos(2\zeta) \\ P^S_{+-} &= P^S_{-+} = \Delta\sin(2\zeta) \end{aligned} \tag{7}$$

where $\Sigma = \frac{1}{2}(p_1 + p_2)$ and $\Delta = \frac{1}{2}(p_1 - p_2)$. Using eqn (1) and omitting *Z*, the contribution of these two levels to the singlet yield is:

$$\Phi_S^{\pm} = \left(P_{++}^S\right)^2 + \left(P_{--}^S\right)^2 + 2\left(P_{+-}^S\right)^2 \frac{k^2}{k^2 + 4\left(a^2q^2 + b^2\right)}. \tag{8}$$

Combining eqn (8) with eqn (7) and subtracting the singlet yield in the absence of an avoided crossing, we obtain:

$$\Phi_S^{\pm} - \Phi_S^{\pm}(b=0) = \frac{-8b^2\Delta^2}{k^2 + 4b^2 + 4a^2q^2}. \tag{9}$$

This is a negative Lorentzian function of *q*, centred at the position of the avoided crossing ($q = 0$) with amplitude

$$\frac{-8b^2\Delta^2}{k^2 + 4b^2} \tag{10}$$

and full width at half maximum height

$$\sqrt{\frac{4b^2 + k^2}{a^2}}. \tag{11}$$

It is clear from eqns (10) and (11), that as the lifetime of the radical pair is prolonged (by reducing *k*), the spike becomes stronger and narrower with the height and width tending to $-2\Delta^2$ and $2b/a$, respectively, in the limit *k* << 2*b*. In the opposite limit, *k* >> 2*b*, the spike vanishes. The other conditions for the existence of a spike in this simple model are that there is an avoided crossing ($b \neq 0$) and that the basis states have different singlet characters ($\Delta \neq 0$).

The condition, derived above, that the two energy levels involved in the avoided crossing must have different singlet characters may be used to deduce a condition on the counter-radical. Writing the pair of interacting states as

$$|\psi_1\rangle = |\phi_A\rangle|\phi_B\rangle \quad \text{and} \quad |\psi_2\rangle = |\phi'_A\rangle|\phi_B\rangle, \tag{11}$$

where A and B label the two radicals, we have:

$$\langle\psi_1|\hat{P}^S|\psi_1\rangle - \langle\psi_2|\hat{P}^S|\psi_2\rangle = \sum_{q=x,y,z}\left[\langle\phi_A|\hat{S}_{Aq}|\phi_A\rangle - \langle\phi'_A|\hat{S}_{Aq}|\phi'_A\rangle\right]\langle\phi_B|\hat{S}_{Bq}|\phi_B\rangle. \tag{11}$$

With a simple "crossing" Hamiltonian for radical A containing a single spin-$\frac{1}{2}$ nucleus (axial hyperfine interaction, $A_{xx} = A_{yy} = 0$, and the magnetic field perpendicular to the hyperfine axis):

$$\hat{H}_A = \gamma_e B_0 \hat{S}_{Ax} + A_{zz}\hat{S}_{Az}\hat{I}_z \tag{11}$$

it can be shown that

$$\langle\psi_1|\hat{P}^S|\psi_1\rangle - \langle\psi_2|\hat{P}^S|\psi_2\rangle \propto \langle\phi_B|\hat{S}_{Bz}|\phi_B\rangle \tag{11}$$

That is, for an avoided crossing to give a spike in Φ_S, we require the *z*-component of the electron spin in the counter-radical to be non-zero.

S9. Simplified FAD-containing radical pairs

Fig. S4 shows the simulations for [$FAD^{\bullet-}$ $Y^{\bullet}$] referred to in the sub-section *Simpler flavin-containing radical pairs* in the main text. A spike is not seen unless the hyperfine tensor of the single (^{14}N) nucleus in $Y^{\bullet}$ is anisotropic. The spikes at θ = 90° arise from $FAD^{\bullet-}$ (as discussed in the text). The additional spikes at θ = 45° come from $Y^{\bullet}$.

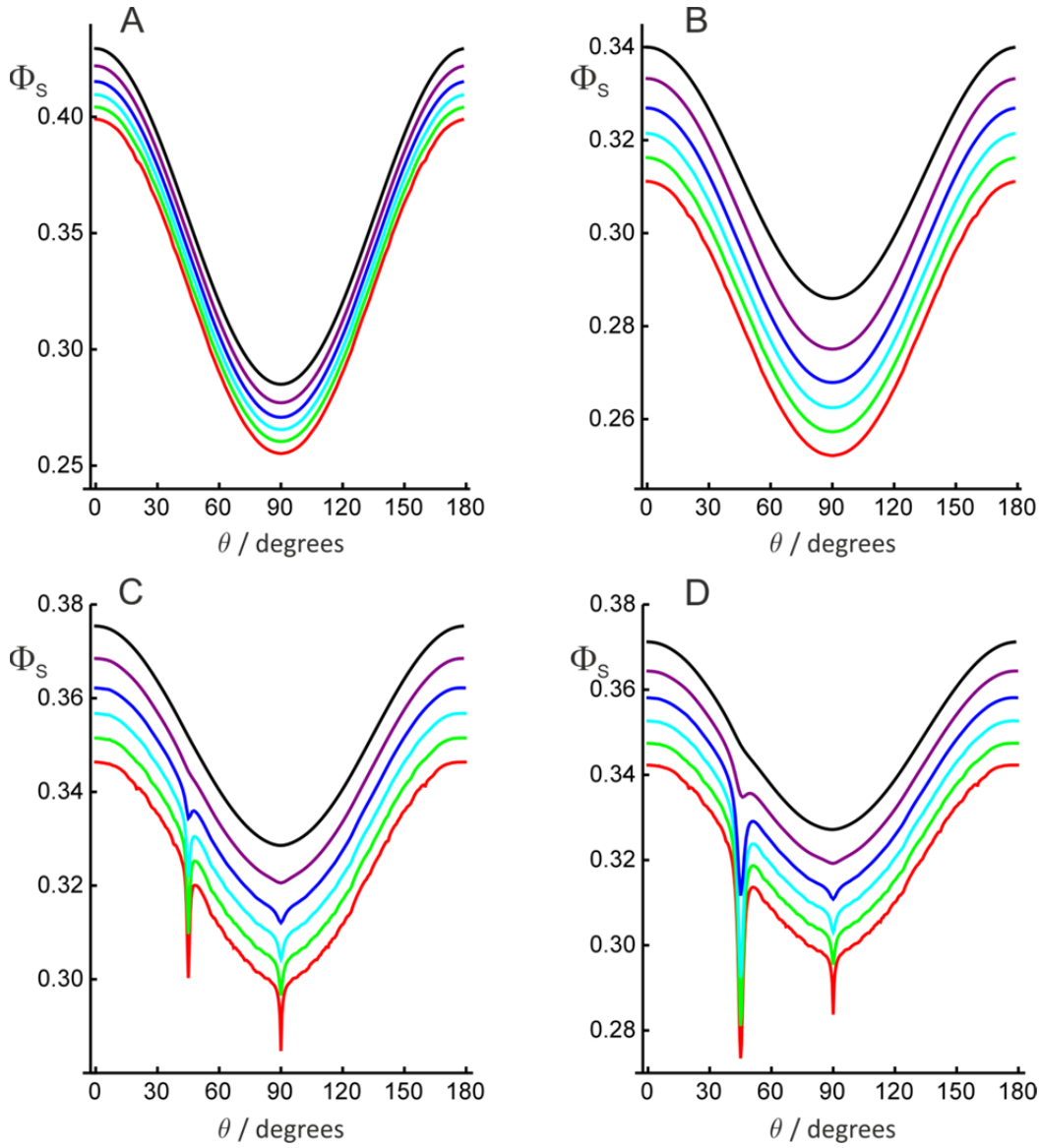

Fig. S4. Φ_S for a [$FAD^{\bullet-}$ $Y^{\bullet}$] radical pair in which radical $Y^{\bullet}$ contains a single ^{14}N nucleus. The radical pair lifetimes are as in Fig. 2B: black 1 μs, purple 2 μs, blue 5 μs, cyan 10 μs, green 20 μs, red 100 μs. The angle between the *z*-axes of $Y^{\bullet}$ and $FAD^{\bullet-}$ was 45°. For clarity, the five traces for τ < 100 μs have been offset vertically, from top to bottom, by 0.020, 0.016, 0.012, 0.008, and 0.004 respectively. The hyperfine tensors of the ^{14}N nucleus in $Y^{\bullet}$ were:

A. (A_{xx}, A_{yy}, A_{zz}) = (0.0, 0.0, 0.0)
B. (A_{xx}, A_{yy}, A_{zz}) = (0.3604, 0.3604, 0.3604) mT (isotropic)
C. (A_{xx}, A_{yy}, A_{zz}) = (–0.1, –0.1, 1.2812) mT (axial)
D. (A_{xx}, A_{yy}, A_{zz}) = (–0.2, 0.0, 1.2812) mT (rhombic)

S10. Calculation of Φ_S for radicals undergoing rotational jumps

The simulations in Fig. 3 in the main text were carried out as follows. The density operator $\rho(t)$ of a radical pair in a singlet state at time t was obtained from the Liouville equation:

$$\frac{\mathrm{d}\hat{\rho}}{\mathrm{d}t} = -\hat{\hat{L}}\hat{\rho} \;\Rightarrow\; \hat{\rho}(t) = \mathrm{e}^{-\hat{\hat{L}}t}\hat{\rho}(0) = \frac{1}{Z}\mathrm{e}^{-\hat{\hat{L}}t}\hat{P}^{\mathrm{S}}$$

in which $\hat{P}^{\mathrm{S}}$ is the singlet projection operator, Z is the number of nuclear spin configurations and the $\hat{\hat{L}}$ is the Liouvillian superoperator . The fraction of radical pairs in the singlet state, $p_{\mathrm{S}}(t)$, is:

$$p_{\mathrm{S}}(t) = \mathrm{Tr}\left[\hat{P}^{\mathrm{S}}\hat{\rho}(t)\right] = \frac{1}{Z}\mathrm{Tr}\left[\hat{P}^{\mathrm{S}}\mathrm{e}^{-\hat{\hat{L}}t}\hat{P}^{\mathrm{S}}\right]$$

and the yield of the reaction product formed from the singlet state is:

$$\Phi_{\mathrm{S}} = k\int_0^{\infty} p_{\mathrm{S}}(t)\mathrm{d}t = \frac{k}{Z}\mathrm{Tr}\left[\hat{P}^{\mathrm{S}}\hat{\hat{L}}^{-1}\hat{P}^{\mathrm{S}}\right]$$

in which k is the recombination rate constant for singlet and triplet states ($k = \tau^{-1}$). L and ρ, the matrix representations of $\hat{\hat{L}}$ and $\hat{\rho}$ respectively, were constructed from the matrix representations of the Liouvillians and density operators for the two sites, $L_{\pm}$ and $\rho_{\pm}$:

$$L = \begin{pmatrix} L_{+} + k_{\mathrm{r}}E & -k_{\mathrm{r}}E \\ -k_{\mathrm{r}}E & L_{-} + k_{\mathrm{r}}E \end{pmatrix} \quad \text{and} \quad \rho = \begin{pmatrix} \rho_{+} \\ \rho_{-} \end{pmatrix}$$

where k_{r} is the rocking rate constant. E is the identity matrix. $L_{\pm}$ have dimension $4Z^2$. $\rho_{\pm}$ are column vectors with the same dimension. $L_{\pm}$ were obtained from the corresponding spin Hamiltonians:

$$L_{\pm} = \mathrm{i}\left[H_{\pm}\otimes E - E\otimes H_{\pm}^{\mathrm{T}}\right] + kE$$

with (see Section S5):

$$\hat{H}_{\pm} = \gamma_{\mathrm{e}}B_0\left[\left(\hat{S}_{\mathrm{A}x}+\hat{S}_{\mathrm{B}x}\right)\sin\theta\cos\phi + \left(\hat{S}_{\mathrm{A}y}+\hat{S}_{\mathrm{B}y}\right)\sin\theta\sin\phi + \left(\hat{S}_{\mathrm{A}z}+\hat{S}_{\mathrm{B}z}\right)\cos\theta\right]$$
$$+\sum_{n=1}^{N_{\mathrm{A}}} a_{\mathrm{A}n}^{\mathrm{iso}}\hat{\mathbf{S}}_{\mathrm{A}}.\hat{\mathbf{I}}_{\mathrm{A}n} + \sum_{m=1}^{N_{\mathrm{B}}} a_{\mathrm{B}m}^{\mathrm{iso}}\hat{\mathbf{S}}_{\mathrm{B}}.\hat{\mathbf{I}}_{\mathrm{B}m} + \sum_{n=1}^{N_{\mathrm{A}}}\hat{\mathbf{S}}_{\mathrm{A}}.\mathbf{R}_{\pm}^{-1}.\mathbf{T}_{\mathrm{A}n}.\mathbf{R}_{\pm}.\hat{\mathbf{I}}_{\mathrm{A}n} + \sum_{m=1}^{N_{\mathrm{B}}}\hat{\mathbf{S}}_{\mathrm{B}}.\mathbf{T}_{\mathrm{B}m}.\hat{\mathbf{I}}_{\mathrm{B}m}$$

The matrices that rotate radical A between the two sites are given by:

$$\mathbf{R}_{\pm} = \cos\beta\mathbf{E} \pm \sin\beta\begin{pmatrix} 0 & -u_z & u_y \\ u_z & 0 & -u_x \\ -u_y & u_x & 0 \end{pmatrix} + (1-\cos\beta)\begin{pmatrix} u_x^2 & u_xu_y & u_xu_z \\ u_xu_y & u_y^2 & u_yu_z \\ u_xu_z & u_yu_z & u_z^2 \end{pmatrix}$$

where the unit vector (u_x, u_y, u_z) is the rotation axis and β is the rotation angle.

S11. Amplitudes and widths of the spike for radicals undergoing rotational jumps

To obtain a more quantitative picture of the way in which the spike is affected by two-site hopping, the singlet yields in Fig. 3A for the toy radical pair were fitted to a function of the form:

$$a + b\cos^2\theta - \frac{Hw^2}{(\theta-\theta_0)^2 + w^2} .$$

That is, the rolling background was approximately modelled as $a + b\cos^2\theta$ and the spike by an inverted Lorentzian of amplitude H, width $2w$, centred at $\theta = \theta_0$. The dependence of H (left) and w (right) on the hopping rate constant are shown in Fig. S5, together with the values for the static case with no hopping (extreme right hand side of each plot). While the amplitude drops as the hopping becomes slower, there is hardly any change in the width.

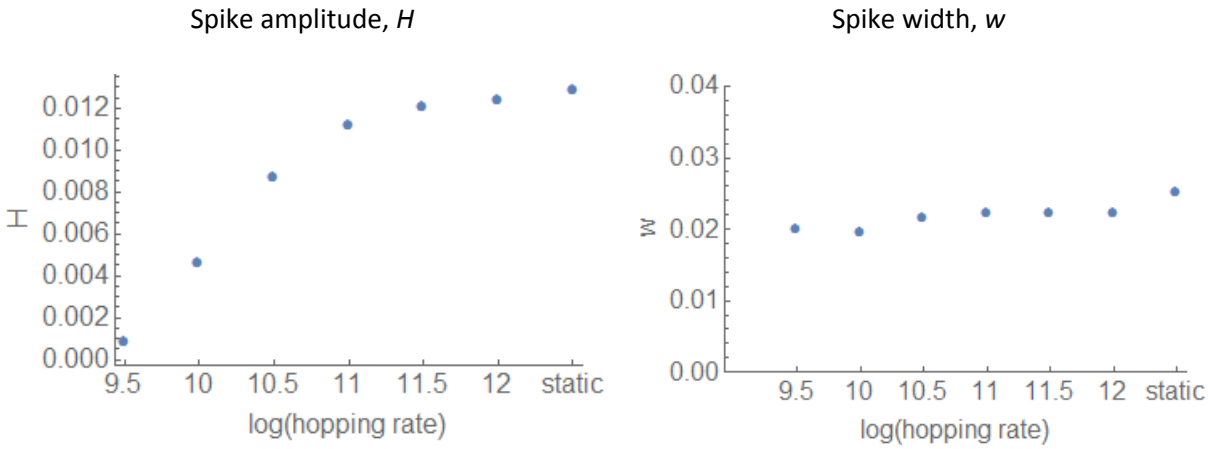

Fig. S5. Variation of the amplitude and width of the spike in Fig. 3A with rate constant k_r.

S12. Φ_S for [X$^\bullet$ Y$^\bullet$] radical pair undergoing slow rotational jumps

Fig. S6 compares Fig. 3A from the main text (3×10^{11} s$^{-1} \geq k_r \geq 1 \times 10^8$ s^{-1} (reproduced here as Fig. S6A) with the corresponding simulations for 1×10^8 s$^{-1} \geq k_r \geq 1 \times 10^5$ s^{-1} (Fig. S6B). Sharp spikes are seen when the rocking is either fast ($k_r \geq 3 \times 10^9$ s^{-1}) or slow ($k_r \leq 3 \times 10^6$ s^{-1}).

In the intermediate regime (10^7 s$^{-1} \leq k_r \leq 10^9$ s^{-1}), where k_r is comparable to the strengths of the hyperfine interactions, spin relaxation is fast and results in attenuation of both the spike and the broad background. The loss of spin-correlation is most efficient when $k_r \approx 1 \times 10^8$ s^{-1}, with Φ_S tending towards 0.25, the statistical singlet fraction expected for an equilibrated radical pair.

As the value of k_r is reduced from 1×10^8 s^{-1} (Fig. S6B), the spike at $\theta = 90°$ reappears when $k_r = 3 \times 10^6$ s^{-1} and splits into two (at $\theta = 90 \pm 5°$) when $k_r \leq 3 \times 10^5$ s^{-1}, corresponding to static disorder on the timescale of the radical pair lifetime, τ.

In principle, the pair of sharp spikes seen for the slowest rocking rates in Fig. S6B ($k_r \leq 3 \times 10^5$ s^{-1}) could afford directional information. However it is not likely that a radical would, in reality, jump between just two well-defined orientations. More realistically, there would be a distribution of thermally accessible orientations so that, in the slow motion limit, the spike would be broadened to an extent that reflected the static distribution of internal magnetic interactions. A sharp spike and precise directional information are therefore much more likely to be found in the fast motion regime ($k_r \geq 3 \times 10^9$ s^{-1} in Fig. S6A).

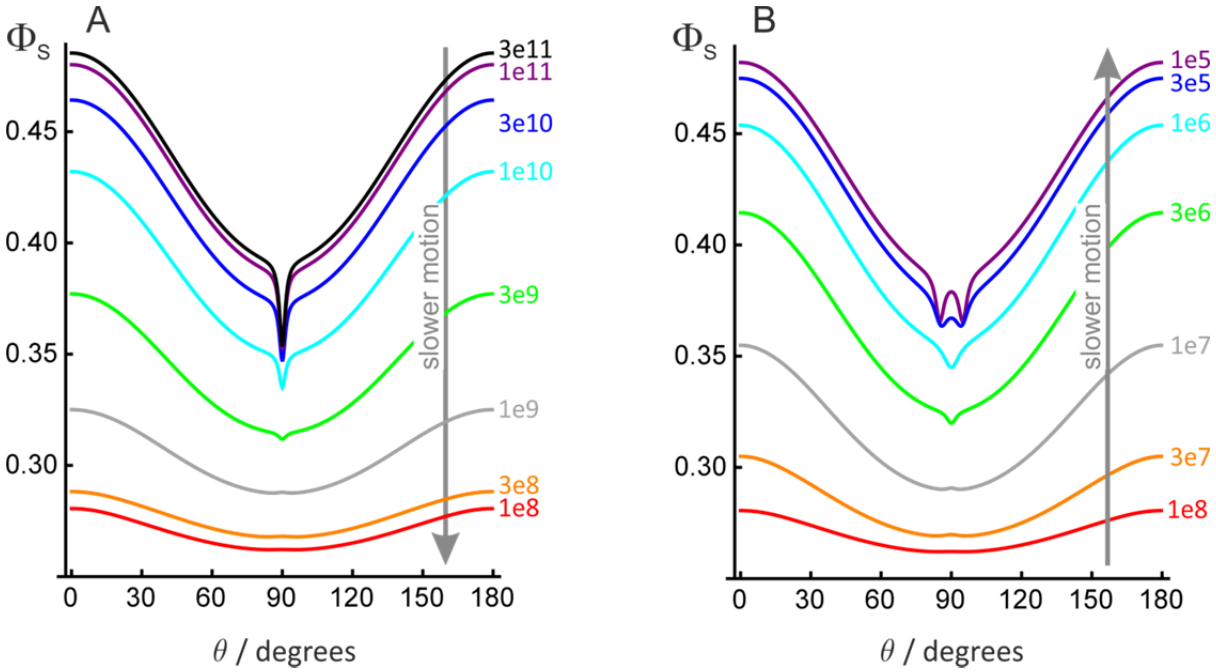

Fig. S6. Φ_S for the toy radical pair, [X$^\bullet$ Y$^\bullet$]. X$^\bullet$ has a single ^{14}N nucleus with hyperfine components (A_{xx}, A_{yy}, A_{zz}) = (–0.2, –0.2, 1.7569) mT; Y$^\bullet$ has a single ^{14}N nucleus with hyperfine components (0.0, 0.0, 1.0812) mT. The two hyperfine tensors have parallel *z*-axes. The radical pair lifetime is 10 μs. X$^\bullet$ underwent 10° jumps (i.e. β = 5°) around the *y*-axis with rate constants k_r (A) between 3×10^{11} s^{-1} and 1×10^8 s^{-1} and (B) between 1×10^8 s^{-1} and 1×10^5 s^{-1}, as indicated.

We have modelled the spin relaxation that arises from modulation of the hyperfine interactions by librational motions of the radicals within the protein. An additional source of relaxation is the time-dependence of the electron-electron exchange and dipolar interactions arising from fluctuations in the radical-radical separation. Interestingly, this relaxation mechanism can boost the anisotropy of Φ_S by relaxing the spins more efficiently for some directions of the magnetic field than for others. This will be the subject of a future publication.

S13. Φ_S for [X$^{\bullet}$ TrpH$^{\bullet+}$] radical pair in which TrpH$^{\bullet+}$ undergoes rotational jumps

Fig. 3B from the main text (reproduced here as Fig. S7A) shows simulations for a [FAD$^{\bullet-}$ Y$^{\bullet}$] radical pair including the spin relaxation that results from the FAD$^{\bullet-}$ radical undergoing 10° rotational jumps (i.e. $\beta = 5°$). Fig. S7B shows the corresponding simulations for a [X$^{\bullet}$ TrpH$^{\bullet+}$] radical pair in which the TrpH$^{\bullet+}$ radical undergoes the same rotational jumps.

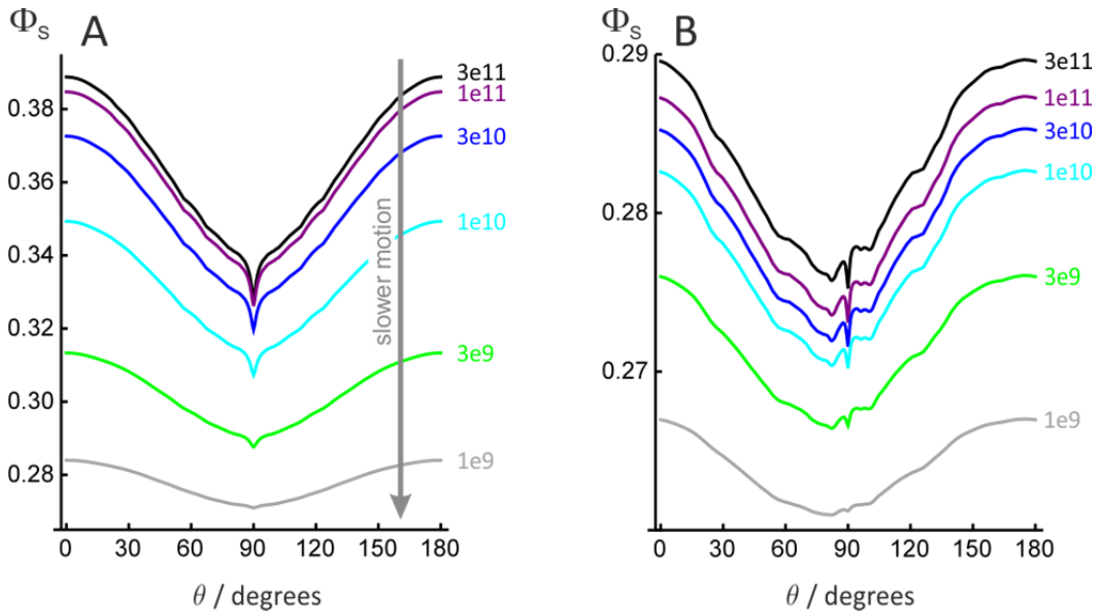

Fig. S7. Φ_S for (A) a [FAD$^{\bullet-}$ Y$^{\bullet}$] and (B) a [X$^{\bullet}$ TrpH$^{\bullet+}$] radical pair with the FAD$^{\bullet-}$ and TrpH$^{\bullet+}$ radicals undergoing 10° rotational jumps (i.e. $\beta = 5°$). Y$^{\bullet}$ has a single ^{14}N nucleus with hyperfine components (A_{xx}, A_{yy}, A_{zz}) = (0.0, 0.0, 1.0812) mT. X$^{\bullet}$ has a single ^{14}N nucleus with hyperfine components (A_{xx}, A_{yy}, A_{zz}) = (–0.1002, –0.0868, 1.7569) mT. In both cases, the radical pair lifetime was 10 μs. The rate constants (k_r) for the rocking motion are: black 3×10^{11} s^{-1}, purple 1×10^{11} s^{-1}, blue 3×10^{10} s^{-1}, cyan 1×10^{10} s^{-1}, green 3×10^{9} s^{-1}, grey 1×10^{9} s^{-1}.

S14. Precision of compass bearing

A rough idea of the precision of the compass bearing available from any given $\Phi_S(\theta)$ ($0 \leq \theta \leq 180°$) may be obtained as follows by considering the effect of stochastic detector noise. $\Phi_S(\theta)$ was calculated for a range of values of θ; random numbers, drawn from a Gaussian distribution with mean 0.0 and standard deviation σ, were added to give a noisy 'signal', $\tilde{\Phi}_S(\theta)$. The compass bearing available from $\tilde{\Phi}_S(\theta)$ was taken to be $\tilde{\theta}$, the value of θ corresponding to the minimum value of $\tilde{\Phi}_S(\theta)$. If the signal-to-noise ratio is not too low, $\tilde{\theta}$ should be close to 90° for the (noise-free) signals in Fig. 1B. The calculation was repeated 10^4 times with the same $\Phi_S(\theta)$ and a fresh set of random noise each time, drawn from the same Gaussian distribution. The uncertainty in the compass bearing, Ξ, is defined as the standard deviation of the 10^4 values of $\tilde{\theta}$. One can expect that a sharper and stronger spike will deliver a more precise compass bearing and consequently a smaller value of Ξ. Similarly, the lower the noise level, σ, the smaller Ξ should be.

To compare the performance of [$FAD^{\bullet-}$ $TrpH^{\bullet+}$] for different lifetimes under the conditions of Fig. 1, we determined, for each value of τ, the amount of noise (σ) that could be introduced before Ξ exceeded 1°. The results are shown in Table S5.

Table S5. Values of the noise level σ that would allow direction sensing with a precision of 1° using the signals shown in Fig. 1 for [$FAD^{\bullet-}$ $TrpH^{\bullet+}$] with different lifetimes, τ.

τ / μs	1	2	5	10	20	50	100
$10^5\sigma$	1.1	8.7	29	44	61	86	104
σ_{rel}♥	1.0	7.9	26.5	40.2	55.8	78.3	95.2
S/*N*♠	90.5	19.6	10.3	9.2	8.5	7.9	7.7

♥ σ_{rel} is the value of σ relative to that when $\tau = 1$ μs.

♠ The signal-to-noise ratio, *S*/*N*, was obtained from *S* = $\max\left[\Phi_S(\theta)\right] - \min\left[\Phi_S(\theta)\right]$ and *N* = σ.

S15. References

1. Frisch MJ*, et al.* (2004) Gaussian 03 (Gaussian, Inc., Wallingford, CT), revision C.02.
2. Rodgers CT (2007) D. Phil. thesis, University of Oxford.
3. Zoltowski BD*, et al.* (2011) Structure of full-length *Drosophila* cryptochrome. *Nature* 480(7377):396-399.
4. Levy C*, et al.* (2013) Updated structure of *Drosophila* cryptochrome. *Nature* 495:E3-E4.
5. Efimova O & Hore PJ (2008) Role of exchange and dipolar interactions in the radical pair model of the avian magnetic compass. *Biophys. J.* 94(5):1565-1574.
6. Müller P, Yamamoto J, Martin R, Iwai S, & Brettel K (2015) Discovery and functional analysis of a 4th electron-transferring tryptophan conserved exclusively in animal cryptochromes and (6-4) photolyases. *Chem. Commun.* 51(85):15502-15505.
7. Timmel CR, Till U, Brocklehurst B, McLauchlan KA, & Hore PJ (1998) Effects of weak magnetic fields on free radical recombination reactions. *Mol. Phys.* 95(1):71-89.
8. Cintolesi F, Ritz T, Kay CWM, Timmel CR, & Hore PJ (2003) Anisotropic recombination of an immobilized photoinduced radical pair in a 50-µT magnetic field: a model avian photomagnetoreceptor. *Chem. Phys.* 294(3):385-399.
9. Till U, Timmel CR, Brocklehurst B, & Hore PJ (1998) The influence of very small magnetic fields on radical recombination reactions in the limit of slow recombination. *Chem. Phys. Lett.* 298(1-3):7-14.
10. Ritz T, Adem S, & Schulten K (2000) A model for photoreceptor-based magnetoreception in birds. *Biophys. J.* 78(2):707-718.
11. Ritz T, Ahmad M, Mouritsen H, Wiltschko R, & Wiltschko W (2010) Photoreceptor-based magnetoreception: optimal design of receptor molecules, cells, and neuronal processing. *J. Roy. Soc. Interface* 7:S135-S146.
12. Lau JCS, Rodgers CT, & Hore PJ (2012) Compass magnetoreception in birds arising from photo-induced radical pairs in rotationally disordered cryptochromes. *J. Roy. Soc. Interface* 9:3329-3337.
13. Solov'yov IA, Mouritsen H, & Schulten K (2010) Acuity of a cryptochrome and vision-based magnetoreception system in birds. *Biophys. J.* 99(1):40-49.
14. Niessner C*, et al.* (2011) Avian ultraviolet/violet cones identified as probable magnetoreceptors. *Plos One* 6(5):e20091.
15. Lau JCS (2013) D. Phil. thesis, University of Oxford.
16. Eriksson LEG & Ehrenberg A (1973) Powder ESR and ENDOR spectra of flavoprotein radicals. *Biochim. Biophys. Acta* 295(1):57-66.
17. Martinez JI, Alonso PJ, & Medina M (2012) The electronic structure of the neutral isoalloxazine semiquinone within *Anabaena* flavodoxin: New insights from HYSCORE experiments. *J. Magn. Reson.* 218:153-162.
18. Martinez JI, Alonso PJ, Gomez-Moreno C, & Medina M (1997) One- and two-dimensional ESEEM spectroscopy of flavoproteins. *Biochemistry* 36(49):15526-15537.
19. Barquera B*, et al.* (2003) X- and W-band EPR and Q-band ENDOR studies of the flavin radical in the Na^+-translocating NADH : quinone oxidoreductase from *Vibrio cholerae*. *J. Am. Chem. Soc.* 125(1):265-275.
20. Weber S, Mobius K, Richter G, & Kay CWM (2001) The electronic structure of the flavin cofactor in DNA photolyase. *J. Am. Chem. Soc.* 123(16):3790-3798.